Title
Mrx6 regulates mitochondrial DNA copy number in S. cerevisiae

Author
Goke, Aylin

Publication Date
2019

Peer reviewed|Thesis/dissertation

Mrx6 regulates mitochondrial DNA copy number in S. cerevisiae

by

Aylin Goke

DISSERTATION

Submitted in partial satisfaction of the requirements for degree of

DOCTOR OF PHILOSOPHY

in

Biochemistry and Molecular Biology

in the

GRADUATE DIVISION

of the

UNIVERSITY OF CALIFORNIA, SAN FRANCISCO

Approved:

Peter Walter — Peter Walter

Chair

David Morgan — David Morgan

Wallace Marshall — Wallace Marshall

Jodi Nunnari

Committee Members

I dedicate this dissertation to my parents,

Yusuf Ziya and Zehra Lerzan Göke.

Acknowledgments

I am grateful to the people who participated in this work and supported me along this journey. I first want to thank Peter Walter for giving me the opportunity to study an intriguing question in his lab. I am really grateful for his mentorship throughout my research and his invaluable support, scientifically and otherwise. Special thanks to my thesis committee, Jodi Nunnari, David Morgan, Wallace Marshall, and other UCSF faculty, Patrick O'Farrell and Carol Gross for their technical advice, guidance and insightful discussions. I am also grateful to Christof Osman for his mentorship and tremendous help. I want to thank every member of the Walter Lab; this work would not have been possible without their help and support.

I also want to thank my college friends, Özge Vargel, Fatih Mehmet Bölükbasi and Arda Mizrak, and my undergraduate mentor Ebru Erbay. Even though they were far away, they were always available for me when I needed them. I want to thank Alexander Green who bore with me all the time, proof-read whatever I have written and constantly reminded me to laugh. Finally, I want to thank my parents, Zehra Lerzan and Yusuf Ziya Göke, and my brother Gökhan Göke, for giving me the tremendous support and encouragement I needed to complete my degree.

Contributions

People who contributed to the research that forms the basis for the thesis:

Aylin Göke: Conceptualization, Data curation, Formal analysis, Validation, Investigation, Visualization, Methodology, Writing—original draft, Writing—review and editing;

Arda Mizrak: Conceptualization, Formal analysis, Software;

Vladislav Belyy: Conceptualization, Formal analysis, Software, Supervision, Writing—review and editing;

Christof Osman: Conceptualization, Data curation, Formal analysis, Validation, Investigation, Visualization, Methodology, Software, Supervision, Writing—review and editing;

Peter Walter: Conceptualization, Funding acquisition, Resources, Supervision, Writing—review and editing.

Mrx6 regulates mitochondrial DNA copy number in *S. cerevisiae*

Aylin Göke

Abstract

Mitochondria carry their own genome (mtDNA), which is present in multiple copies in all eukaryotic cells. Copy number of mtDNA in each cell is tightly maintained, yet surprisingly the cellular mechanisms that regulate mtDNA copy number remain poorly understood. To address this question, we carried out a forward genetic screen in the budding yeast *S. cerevisiae* and identified mutants exhibiting altered mtDNA levels. This screen revealed a previously uncharacterized mitochondrial gene, *Mrx6*, whose deletion results in a marked increase of mtDNA without affecting mitochondrial structure or cell size. We found that Mrx6 forms a complex with a sequence-related protein, Pet20, with Mam33, and with the conserved Lon protease Pim1, which is important for mitochondrial protein quality control. Furthermore, the Mrx6 complex colocalizes with mtDNA. Because human and bacterial Lon proteases have been proposed to regulate DNA replication by degrading replication initiation factors, our results suggest that the Mrx6 complex may similarly control mtDNA levels through degradation of key proteins regulating mtDNA replication.

Table of Contents

List of Figures

List of Tables

CHAPTER I

Introduction: mtDNA copy number control

Mitochondria are endosymbiotic organelles that carry multiple copies of their own genome, encoding proteins required for oxidative phosphorylation and respiratory metabolism. mtDNA copies are packaged together with several mtDNA binding proteins to form nucleoids that distribute throughout the mitochondrial network and display a semi-regular spacing (Brown et al., 2011; Chen and Butow, 2005; Jajoo et al., 2016; Lewis et al., 2016; Osman et al., 2015). The copy number of mtDNA in each cell is maintained within a narrow range (Chen and Butow, 2005; Clay Montier et al., 2009). Previous studies reported that *S. cerevisiae* cells maintain ~40-60 nucleoids, each carrying ~1-2 mtDNA copies (Chen and Butow, 2005), although some reviews cite up to 10 copies per nucleoid (Lipinski et al., 2010). Mammalian cells can contain thousands of nucleoids, which vary depending on tissue type (Miller et al., 2003; Williams, 1986), and each nucleoid contains a single mtDNA copy (Kukat et al., 2015). Altered levels of mtDNA are linked to a variety of diseases, including neurodegenerative and metabolic diseases and various types of cancer (Clay Montier et al., 2009; Pyle et al., 2016; Ylikallio et al., 2010; Yu, 2011). Furthermore, increasing mtDNA copy number has been suggested to help cells to ameliorate the effect of myocardial infarction in mice (Ikeda et al., 2015). Despite their physiological importance, the cellular mechanisms that regulate mtDNA copy number remain poorly understood.

A similar phenomenon is found in maintenance of multiple copy plasmids in prokaryotes. In these systems, copy number of plasmids is primarily controlled at the level of initiation of plasmid DNA replication by plasmid encoded factors (activators/inhibitors of DNA replication, controlling primer synthesis by plasmid encoded RNAs), as well as host encoded modulators (Paulsson and Chattoraj, 2006; del Solar et al., 1998). Thus, cells maintain sufficient amount of plasmids for stable inheritance, avoids excess accumulation, and modulates copy number depending on different conditions. One question is whether there is an analogous regulation of mtDNA replication to maintain the copy number at its physiological level.

Previously, dNTP pools and proteins regulating ribonuclease reductase activity were implicated to regulate mtDNA levels (Taylor et al., 2005). Similarly, the mtDNA packaging protein and transcription factor TFAM in human cells, and its ortholog Abf2 in yeast were shown to modulate mtDNA copy number (Ekstrand et al., 2004 ; Zelenaya-Troitskaya et al., 1998). Moreover, increasing levels of mtDNA helicase Twinkle in human cells increased mtDNA levels (Ikeda et al., 2015). However, while these players are all involved with mtDNA homeostasis, their role in maintaining mtDNA copy number is unclear.

Previous genetic screens designed to identify new components that control mtDNA copy number focused on mutants that lead to mtDNA loss and identified numerous components important for mtDNA maintenance (Fukuoh et al., 2014; Zhang and Singh, 2014). However, loss of mtDNA is often caused by secondary effects due to compromised mitochondrial function (Lipinski et al., 2010). Therefore, the question of how mtDNA copy number is regulated to remain within a narrow window has remained largely unanswered. To begin addressing the gap in our knowledge, we developed a genetic screen in the budding yeast *S. cerevisiae*, designed to comprehensively identify genes that are required to sustain mtDNA levels at their physiological set-point.

References

Brown, T.A., A.N. Tkachuk, G. Shtengel, B.G. Kopek, D.F. Bogenhagen, H.F. Hess, and D.A. Clayton. 2011. Superresolution fluorescence imaging of mitochondrial nucleoids reveals their spatial range, limits, and membrane interaction. *Mol Cell Biol*. 31:4994-5010.

Chen, X.J., and R.A. Butow. 2005. The organization and inheritance of the mitochondrial genome. *Nat Rev Genet*. 6:815-825.

Clay Montier, L.L., J.J. Deng, and Y. Bai. 2009. Number matters: control of mammalian mitochondrial DNA copy number. *J Genet Genomics*. 36:125-131.

del Solar, G., R. Giraldo, M.J. Ruiz-Echevarría, M. Espinosa, R. Díaz-Oreja. 1998. Replication and control of circular bacterial plasmids. *Microbiology and molecular biology reviews.* 62(2): 434-64.

Ekstrand, M.I., M. Falkenberg, A. Rantanen, C.B. Park, M. Gaspari, K. Hultenby, P. Rustin, C.M. Gustafsson, and N.G. Larsson. 2004. Mitochondrial transcription factor A regulates mtDNA copy number in mammals. *Hum Mol Genet*. 13:935-944.

Fukuoh, A., G. Cannino, M. Gerards, S. Buckley, S. Kazancioglu, F. Scialo, E. Lihavainen, A. Ribeiro, E. Dufour, and H.T. Jacobs. 2014. Screen for mitochondrial DNA copy number maintenance genes reveals essential role for ATP synthase. *Mol Syst Biol*. 10:734.

Ikeda, M., T. Ide, T. Fujino, S. Arai, K. Saku, T. Kakino, H. Tyynismaa, T. Yamasaki, K. Yamada, D. Kang, A. Suomalainen, and K. Sunagawa. 2015. Overexpression of TFAM or twinkle increases mtDNA copy number and facilitates cardioprotection associated with limited mitochondrial oxidative stress. *PLoS One*. 10:e0119687.

Jajoo, R., Y. Jung, D. Huh, M.P. Viana, S.M. Rafelski, M. Springer, and J. Paulsson. 2016. Accurate concentration control of mitochondria and nucleoids. *Science*. 351:169-172.

Kukat, C., K.M. Davies, C.A. Wurm, H. Spahr, N.A. Bonekamp, I. Kuhl, F. Joos, P.L. Polosa, C.B. Park, V. Posse, M. Falkenberg, S. Jakobs, W. Kuhlbrandt, and N.G. Larsson. 2015. Cross-strand binding of TFAM to a single mtDNA molecule forms the mitochondrial nucleoid. *Proc Natl Acad Sci U S A*. 112:11288-11293.

Lewis, S.C., L.F. Uchiyama, and J. Nunnari. 2016. ER-mitochondria contacts couple mtDNA synthesis with mitochondrial division in human cells. *Science*. 353:aaf5549.

Lipinski, K.A., A. Kaniak-Golik, and P. Golik. 2010. Maintenance and expression of the S. cerevisiae mitochondrial genome--from genetics to evolution and systems biology. *Biochim Biophys Acta*. 1797:1086-1098.

Miller, F.J., F.L. Rosenfeldt, C. Zhang, A.W. Linnane, and P. Nagley. 2003. Precise determination of mitochondrial DNA copy number in human skeletal and cardiac muscle by a PCR-based assay: lack of change of copy number with age. *Nucleic Acids Res*. 31:e61.

Osman, C., T.R. Noriega, V. Okreglak, J.C. Fung, and P. Walter. 2015. Integrity of the yeast mitochondrial genome, but not its distribution and inheritance, relies on mitochondrial fission and fusion. *Proc Natl Acad Sci U S A*. 112:E947-956.

Paulsson, J. and D. K. Chattoraj. 2006. Origin inactivation in bacterial DNA replication control. *Molecular Microbiology*, 61: 9-15.

Pyle, A., H. Anugrha, M. Kurzawa-Akanbi, A. Yarnall, D. Burn, and G. Hudson. 2016. Reduced mitochondrial DNA copy number is a biomarker of Parkinson's disease. *Neurobiol Aging*. 38:216 e217-216 e210.

Taylor, S.D., H. Zhang, J.S. Eaton, M.S. Rodeheffer, M.A. Lebedeva, W. O'Rourke T, W. Siede, and G.S. Shadel. 2005. The conserved Mec1/Rad53 nuclear checkpoint pathway regulates mitochondrial DNA copy number in Saccharomyces cerevisiae. *Mol Biol Cell*. 16:3010-3018.

Williams, R.S. 1986. Mitochondrial gene expression in mammalian striated muscle. Evidence that variation in gene dosage is the major regulatory event. *J Biol Chem*. 261:12390-12394.

Ylikallio, E., H. Tyynismaa, H. Tsutsui, T. Ide, and A. Suomalainen. 2010. High mitochondrial DNA copy number has detrimental effects in mice. *Hum Mol Genet*. 19:2695-2705.

Yu, M. 2011. Generation, function and diagnostic value of mitochondrial DNA copy number alterations in human cancers. *Life Sci*. 89:65-71.

Zelenaya-Troitskaya, O., S.M. Newman, K. Okamoto, P.S. Perlman, and R.A. Butow. 1998. Functions of the high mobility group protein, Abf2p, in mitochondrial DNA segregation, recombination and copy number in Saccharomyces cerevisiae. *Genetics*. 148:1763-1776.

Zhang, H., and K.K. Singh. 2014. Global genetic determinants of mitochondrial DNA copy number. *PLoS One*. 9:e105242.

CHAPTER II

A regulator of mtDNA copy number, Mrx6, is identified in *S. cerevisiae* by a forward genetic screen

Results

To identify the cellular machineries that regulate mtDNA levels, we systematically determined the amount of mtDNA relative to nuclear DNA in 5148 strains of a yeast gene-deletion library generated in S288c cells, each lacking a different non-essential gene (*Saccharomyces* Genome Deletion Project). Mutant colonies grown on rich medium were transferred to nylon membranes, lysed, and hybridized with two different sets of fluorescent probes, specific for mtDNA and nuclear DNA respectively (nDNA) (Figs. 1A and B). We determined the fluorescent intensity of both probes and calculated the mtDNA/nDNA ratio for each mutant. Mutants were classified into three categories: 1) mutants that contained an increased mtDNA/nDNA ratio (Fig. 1C, green), 2) mutants that maintained their mtDNA/nDNA ratio similar to wild type cells (WT) (Fig. 1C, yellow), and 3) mutants that lost the majority or all of mtDNA (Fig. 1C, red) (Supp. Fig. 1A; Supp. Table 1). The following observations indicate that this screen faithfully reports on mtDNA levels: ~80% of mutants falling into the third category were previously described to be respiratory-deficient or defective in maintenance of mtDNA (Supp. Fig. 1B; Supp. Table 1.2), and mutants lacking the genes *SML1, RRM3* and *RFX1*, which were previously reported to contain elevated levels of mtDNA (Taylor et al., 2005), were also identified with increased mtDNA/nDNA ratios in our analysis (Supp. Table 1.1).

We henceforth focused on mutants that displayed higher mtDNA/nDNA ratios, which is more likely to be indicative of a defect in mDNA copy number regulation than mutants that have lost mtDNA. To validate our hits, we repeated the colony blot hybridization with the initially identified candidates (167 mutants) and selected 91 mutants for most of which increased mtDNA levels were reproduced for further analysis (Supp. Fig. 1C; Supp. Table 1.3). As yeast colonies on agar plates consist of heterogonous cell populations that differ in their metabolic and respiratory states (Traven et al., 2012), we isolated genomic DNA from the 91 mutants grown in liquid cultures from early-mid logarithmic phase and quantified their mtDNA levels relative to WT cells by quantitative PCR (qPCR). A majority of the mutants (73 of 91) showed an increase in the mtDNA/nDNA ratio of at least a 50% (Supp. Table 1.4).

In yeast, mtDNA copy number linearly correlates with the length of the mitochondrial network (Osman et al., 2015). Furthermore, mitochondrial network volume correlates linearly with cell volume (Rafelski et al., 2012). For this reason, elevated mtDNA levels could result as a secondary effect of increased cell size, as would be expected, for example, in mutants that affect cell cycle progression (Conrad and Newlon, 1982). To eliminate such mutants from our analyses, we determined the cell size of the 91 candidates by flow-cytometry using side-scattered light as a proxy. Indeed, a majority of the mutants showed an increase in cell size (Fig. 1D; Supp. Table 1.4). By contrast, 9 mutants displayed cell sizes that were within 10% of the value obtained for WT cells, making them likely candidates involved in mtDNA copy number regulation (Fig. 1E).

Deletion of an uncharacterized gene, *MRX6*, increases mtDNA copy number

From the genes whose deletion resulted in increased mtDNA levels without altering cell size, we chose to focus on *MRX6* for the following reasons: 1) The mtDNA/nDNA ratio increase in Δ*mrx6* cells was the highest among the mutants that do not affect cell size (Fig. 1D), 2) Mrx6 has a predicted mitochondrial targeting sequence, and 3) Mrx6 belongs to an uncharacterized protein family. To verify that increased levels of mtDNA are linked to deletion of *MRX6* (and are not caused by second-site mutation in the library strain), we engineered a fresh Δ*mrx6* deletion strain, which reproduced the phenotype of strongly elevated mtDNA levels (Fig. 2A). While we observed a ~2.5 fold increase in the library strain, we observed only a ~1.5 fold increase in the newly generated strain. We attribute this difference to the fact that both strains were generated in different yeast backgrounds (S288c vs. W303), carrying different amount of mtDNA (Connelly and Akey, 2012), and/or possible aggravating second site mutations in the library strain. The 1.5-fold increase in Δ*mrx6* cells versus WT cells was statistically significant ($p<0.01$). For the remaining experiments, we used the freshly generated Δ*mrx6* W303 strain.

Previous studies reported that mtDNA abundance ranges from 25 to 100 copies per cell depending on the strain and growth conditions (Chen and Butow, 2005; MacAlpine et al., 2000). To obtain an accurate quantification of mtDNA levels in our strains, we determined the absolute mtDNA copy number by qPCR analysis using oligo nucleotides specific for nuclearly encoded *ACT1* and mitochondrially encoded *COX1*. To this end, we cloned ~1 kb fragments of *ACT1* and *COX1* into plasmids, which we used as standards to correlate threshold PCR cycle values to copy number. According to these measurements, we conclude that haploid WT cells have 21 (± 4) copies of mtDNA, whereas Δ*mrx6* cells carry 32 (± 5) copies (Fig. 2A), confirming our finding that deletion of *MRX6* increases mtDNA copy number.

We next tested whether deletion of *MRX6* compromises the integrity of mitochondria. To this end, we monitored growth of Δ*mrx6* cells on a non-fermentable carbon source, which necessitates functional mitochondria. Δ*mrx6* cells did not show any growth phenotype compared to WT cells, suggesting Δ*mrx6* cells maintain their mitochondrial function (Fig. 2B). Next, we tested the Δ*mrx6* phenotype in cells grown under different conditions, such as i) on a non-fermentable carbon source, ii) under oxidizing stress condition, and iii) in the presence of an electron transport chain uncoupler (Figs. 2C and D). These analyses revealed that absence of *MRX6* leads to a robust increase of mtDNA under all conditions tested.

As deletion of *MRX6 increased* mtDNA levels, we next tested whether over-expression of Mrx6 would *decrease* it. To this end, we expressed a C-terminally myc-tagged version of Mrx6 (Mrx6-myc) and validated that it maintained Mrx6 function (Supp. Fig. 2). Over-expression of Mrx6-myc did not alter mtDNA levels (Figs. 2E and F), indicating that cellular levels of Mrx6 are not limiting. Taken together, deletion of *MRX6* increases mtDNA copy number without compromising mitochondrial function, while conversely over-expression of Mrx6 does not affect mtDNA levels.

Deletion of *MRX6* increases mtDNA copy number without altering mitochondrial network length or morphology

To test whether deletion of *MRX6* causes abnormalities in mitochondrial volume or morphology, we visualized the mitochondrial network with a mitochondria-targeted (mt-dsRed) protein in *Δmrx6* and WT cells by fluorescence microscopy (Fig. 3A). We did not detect any changes in mitochondrial morphology (Figs. 3B and C) or network length (Fig. 3D) in *Δmrx6* cells, suggesting that elevated mtDNA levels in *Δmrx6* cells are not a consequence of altered mitochondrial morphology or network length.

To determine copy number of mtDNA in single cells, we used our recently developed mt-LacO-LacI system to visualize mtDNA by fluorescence microscopy. The system is based on an array of LacO repeats integrated into mtDNA, which can be bound by a mitochondria-targeted GFP-tagged LacI protein (Osman et al., 2015). In contrast to our previous work, we applied structured illumination (SI) microscopy on fixed diploid cells to resolve mtDNA copies that are in close proximity to one another (Fig. 3A). We counted ~28 mtDNA copies in WT diploid cells, which is in good agreement with 33 (± 6) mtDNA copies determined by qPCR (Fig. 2A), indicating that the microscopic analysis resolved single mtDNA copies in the majority of cases for WT cells. Given that cells used in this experiment were not synchronized and were going through different stages of cell cycle, resulting in differences in cell size and mitochondrial volume, we compared mtDNA copy number normalized to mitochondrial network length. Deletion of *MRX6* increased the number of mtDNA copies normalized to mitochondrial network length by 1.3-fold (Fig. 3E; WT=1.16, Δ*mrx6*=1.54 mtDNA copies/μm network length). Of note, a 1.3-fold increase is smaller than what we obtained with qPCR (Fig. 2A). We attribute the difference between microscopy and qPCR analysis to the fact that even with SI microscopy, we did not resolve mtDNA copies that are close to one another (such as replicating mtDNA copies). Next, we compared the distances between mtDNA copies along the three-dimensional mitochondrial filament. As a result of increased mtDNA copy number, mtDNA copies in *Δmrx6* cells were closer to each other (mean distance between mtDNA copies are 692 nm and 872 nm for Δ*mrx6* and WT cells, respectively; $p<0.001$; Fig. 3F, in good agreement with the 1.3-fold increase in DNA copy number.) Otherwise, mtDNA copies displayed a semi-regular spacing in Δ*mrx6* cells similar to WT cells.

We next stained fixed diploid cells with DAPI and analyzed them by SI microscopy (Fig. 4A). In contrast to the LacO/LacI system shown above, DAPI stains mtDNA in its entirety rather than just demarking a single locus on it. DAPI staining in WT cells revealed distinct punctate structures known as nucleoids (Meeusen and Nunnari, 2003). While Δ*mrx6* cells showed the same number of nucleoids, the average volume of nucleoids was enlarged ~2.2-fold compared to WT cells (Figs. 4B and C). We verified this finding by using an anti-DNA antibody (Supp. Fig. 3) to ascertain that it was indeed DNA and not other DAPI-stained macromolecules, such as RNA, that gave rise to the increased volume. Notably, nucleoids in Δ*mrx6* cells displayed an oblong shape: their lengths when traced along the mitochondrial network were significantly increased in Δ*mrx6* cells, suggesting that cells lacking *MRX6* display elongated nucleoids (mean length of nucleoids are 430 nm and 630 nm for WT and Δ*mrx6* cells, respectively; $p<0.001$; Supp. Figs. 3A and 3B). Taken together these data show that deletion of *MRX6* increases mtDNA copy number without affecting mitochondrial network length or shape, but alters the spatial organization and shape of nucleoids.

Mrx6 is a member of the PET20-domain containing protein family

Interestingly, Mrx6 contains a PET20-domain of uncharacterized structure and function, which is found in two other mitochondrial proteins, Sue1 and Pet20 in *S. cerevisiae* (Fig. 5A). In addition to the PET20-domain, Mrx6 has a unique C-terminal extension that distinguishes Mrx6 from the rest of the PET20-domain containing proteins (Supp. Fig. 4). To assess whether other PET20-domain containing proteins are important for maintaining mtDNA levels, we deleted the genes encoding these proteins in different combinations and quantified the change of mtDNA levels by qPCR. In line with the colony blots from the initial screen, single deletions of *PET20* or *SUE1* did not alter mtDNA levels significantly. Furthermore, Δ*mrx6* Δ*pet20*, Δ*mrx6* Δ*sue1,* and Δ*mrx6* Δ*pet20* Δ*sue1* double or triple mutant strains displayed elevated levels of mtDNA identical to Δ*mrx6* cells (Fig. 5B). Thus, maintenance of normal mtDNA levels does not depend on Pet20 or Sue1. Similarly, the increase in mtDNA levels in Δ*mrx6* cells does not require Pet20 or Sue1.

Mrx6 forms foci in mitochondria and colocalizes with mtDNA

Mrx6 has a predicted mitochondrial targeting sequence, but to date its localization has not been experimentally determined. We constructed a yeast strain in which we genomically tagged Mrx6 at its endogenous locus with the fluorescent protein mNeonGreen (Mrx6-Neon) to determine its localization by fluorescence microscopy. Cells expressing Mrx6-Neon displayed mtDNA levels indistinguishable from WT cells, indicating that protein function was preserved in the tagged Mrx6 variant (Supp. Fig. 5A). In agreement with its predicted mitochondrial localization, Mrx6-Neon colocalized with mitochondrial matrix-targeted blue fluorescent protein (mtTagBFP), which labels the mitochondrial matrix (Fig. 6A). Interestingly and by contrast to mtTagBFP, Mrx6-Neon formed discrete punctate structures that were non-uniformly distributed along the mitochondrial network.

The punctate localization of Mrx6-Neon was reminiscent of the distribution of mtDNA in the nucleoids in the mitochondrial network. Thus, we next tested whether Mrx6-Neon colocalizes with mtDNA. We stained Mrx6-Neon expressing cells with DAPI and determined Mrx6-Neon and mtDNA localization by microscopy. These analyses revealed that a fraction of Mrx6-Neon puncta colocalized with DAPI signal (Fig. 6B; arrow), whereas others did not (Fig. 6B; asterisk). We quantitatively assessed the proportion of the Mrx6-Neon signal that colocalized with DAPI and *vice versa* by determining the Manders's colocalization coefficient (MCC) between intensity profiles of both fluorescent signals along the mitochondrial network (Figs. 6C and Supp. 5B). The MCC values showed a broad distribution, yet the majority of cells showed ~60% overlap between the two wavelengths, confirming our initial observation of a partial colocalization between Mrx6 and mtDNA (Fig. 6D). Pearson's Correlation Coefficient (PCC) analysis further supported colocalization (Fig. 6E). To further validate these conclusions, we evaluated the significance of the measured MCC and PCC values by comparing our results to a control dataset. This dataset consisted of the same intensity profiles, in which one of the two color channels was randomized (Supp. Fig. 5C). The obtained control MCC and PCC values were consistently lower and showed a significantly different distribution compared to the measured data (Figs. 6D, 6E and Supp. 5D; $p<0.001$). We extended our analysis by comparing the measured MCC and PCC values to a data set in which one of the two channels was shifted against the respective other channel. This analysis further supported our results ($p<0.001$).

Given that only ~60% of the Mrx6-Neon puncta colocalized with nucleoids, it seemed plausible that Mrx6 might still form punctate structures in the absence of mtDNA. To test this possibility, we engineered a rho^0 yeast strain (lacking mtDNA) and expressed Mrx6-Neon and mtTagBFP. Mrx6-Neon still formed puncta in these cells (Fig. 6F). Taken together, Mrx6 localizes to mitochondria and forms puncta that distribute throughout the mitochondrial matrix and partially colocalize with mtDNA. Furthermore, the presence of mtDNA is not strictly necessary for the formation of Mrx6 puncta.

Mrx6 forms a complex with Pet20, Mam33 and Pim1

Next, we aimed to identify interaction partners of Mrx6 to begin getting a molecular understanding about how Mrx6 affects mtDNA levels. To this end, we immunoprecipitated C-terminally Flag-tagged Mrx6 (Mrx6-Flag) and identified interacting proteins by mass spectrometry (MS). Mrx6-Flag preserved Mrx6 function (Supp. Fig. 6). In the MS analyses, the proteins Pim1, Mam33 and, to our surprise, Pet20, co-purified with Mrx6-Flag but were absent in the eluate fraction of control immunoprecipitations from cells that only expressed untagged Mrx6 (Figs. 7A and B).

Pim1 is a highly conserved ATP-dependent mitochondrial Lon protease (Venkatesh et al., 2012), and Mam33 is a specific translational activator of Cox1 mRNA (Roloff and Henry, 2015). We next asked whether, reciprocally, we could co-purify these components by pulling down C-terminally Flag-tagged Pet20 (Pet20-Flag). Strikingly, Mrx6, Pim1 and Mam33 co-purified with Pet20-Flag, thus revealing an interaction network between these four proteins (Fig. 7C). We further examined the interaction hierarchy between these proteins by pulling down Mrx6-Flag from extracts of Δ*pet20* cells. The results showed that Pet20 was dispensable for the interaction between Mrx6-Pim1 and Mrx6-Mam33 (Fig. 7B). By contrast, Pim1-Pet20 and Mam33-Pet20 interactions were drastically reduced in Δ*mrx6* cells*,* suggesting that Mrx6 bridges between Pim1, Mam33, and Pet20 (Fig. 7C).

Since two proteins of the PET20-domain protein family, Mrx6 and Pet20, are found in a protein interaction network together with Pim1 and Mam33, we asked whether the third member of the PET20-domain protein family, Sue1, would show a similar protein interaction profile. To this end, we immunoprecipitated C-terminally Flag-tagged Sue1 (Sue1-Flag). In agreement with the Mrx6-Flag and Pet20-Flag pull-downs that did not identify Sue1, neither Mrx6 nor Pet20 co-immunoprecipitated with Sue1-Flag. However, this experiment revealed that Pim1 also interacts with Sue1 (Fig. 7D). Thus, Pim1 is a common interaction partner of all three PET20-domain containing proteins.

Taken together, these results show that Mrx6, Pet20, Pim1 and Mam33 are part of an interaction network in which Mrx6 is crucial for the complex's architecture, whereas Pet20 is dispensable. In addition, our results support the conclusion that Sue1 forms a separate complex with Pim1, which does not include Mrx6 or Pet20.

Mrx6 partially colocalizes with Pet20 and Pim1

As Mrx6 and Pet20 are part of an interaction network, we next examined the spatial association between them in single cells. To this end, we engineered a yeast strain expressing Mrx6-Neon and C-terminally mRuby-tagged Pet20 (Pet20-Ruby) and performed live-cell microscopy. Pet20-Ruby showed discrete punctate structures along the mitochondrial network similar to Mrx6 (Fig. 8A). Surprisingly, we observed only partial colocalization between Mrx6 and Pet20, in which only some of Mrx6-Neon puncta colocalized with Pet20-Ruby (Fig. 8A; arrow), and *vice versa*. MCC values showed ~50% overlap between Mrx6-Neon and Pet20-Ruby signals (Figs. 8B and Supp. 7A; $p<0.001$), and PCC analysis confirmed their colocalization (Fig. 8C; $p<0.001$).

Since only ~50% of Mrx6 colocalizes with Pet20, we next tested whether Mrx6 would display a similar, partial colocalization with Pim1, a notion suggested by our finding that Pim1 forms a separate complex with Sue1 that lacks Mrx6 or Pet20 (Fig. 7D). Hence, we analyzed the association between Mrx6 and Pim1 using a yeast strain expressing Mrx6-Neon and C-terminally mRuby-tagged Pim1 (Pim1-Ruby), which still preserves protein function (Supp. Fig. 7B). Consistent with Mrx6 and Pet20 colocalization, we again observed partial colocalization between Mrx6 and Pim1 (Fig. 8D). MCC values showed ~50% overlap between Mrx6-Neon and Pim1-Ruby signals (Figs. 8E and Supp. 7C; $p<0.001$), and PCC analysis further supported their colocalization (Fig. 8F; $p<0.001$). Taken together, these data indicate that Mrx6, partially colocalizes with Pet20 and Pim1, suggesting that they form sub-complexes along the mitochondrial network.

The Mrx6 complex colocalizes with mtDNA

We next tested whether colocalization of Mrx6 with Pet20 and Pim1 may preferentially occur in regions close to mtDNA. To this end, we performed triple labeling experiments in which we stained mtDNA with DAPI in cells expressing Mrx6-Neon and Pet20-Ruby. This experiment revealed instances of colocalization between Mrx6-Neon, Pet20-Ruby and mtDNA (Fig. 9A). Because of complexity of images displaying three colors in the confined space of mitochondria, we quantitatively assessed of the degree of colocalization in light of the probability that it might occur by chance. To this end, we binned regions of the Mrx6-Neon and Pet20-Ruby intensity profiles where (1) both proteins colocalized, (2) only Mrx6-Neon but no Pet20-Ruby localized, and (3) only Pet20-Ruby but no Mrx6-Neon localized. We then asked, whether these regions would differentially colocalize with mtDNA. Determination of the MCC values revealed that in Bin 1 (Mrx6-Pet20) on average 77% of the regions colocalized with DAPI (Figs. 9B and Supp. 8A). By contrast, in Bin 2 (Mrx6 only) only 56% of the regions colocalized with DAPI (Bin1 distribution compared to Bin2 $p<0.001$; Fig. 9B), and in Bin 3 (Pet20 only) 42% of the of the regions did so (Bin1 distribution compared to Bin3 $p<0.001$; Supp. Fig. 8A). As a control, we generated a dataset by randomizing the DAPI intensity profile against the Mrx6 and Pet20 profiles and re-calculated the MCC values. Strikingly, the proportion of the Mrx6-Pet20 signal colocalizing with the DAPI signal was reduced to 44% (Figs. 9C and Supp. 8B), matching the colocalization with mtDNA observed for Mrx6 alone (45%; Bin1-Bin2 $p=0.78$; Fig. 9C) or Pet20 alone (44%; Bin1-Bin3 $p=0.79$; Supp. Fig. 8B). These results suggest that Mrx6-Pet20 colocalization preferentially occurs in regions close to mtDNA rather than areas that are devoid of mtDNA.

Finally, we examined the colocalization between Mrx6-Neon, Pim1-Ruby and mtDNA (Fig. 9D). The MCC values revealed that on average 65% of the areas in which Mrx6-Neon and Pim1-Ruby were found together colocalized with the DAPI signal (Figs. 9E and Supp. 8C); whereas only 46% of the Mrx6 signal ($p<0.001$; Fig. 9E), and 36% of the Pim1 signal colocalized with the DAPI signal when they were alone ($p<0.001$; Supp. Fig. 8C). Moreover, the percentage of the Mrx6-Pim1 signal colocalizing with the randomized DAPI signal reduced to 38% (Figs. 9F and Supp. 8D), closely matching the values for Mrx6 alone (37%; $p=0.49$; Fig. 9F) and Pim1 alone (38%; $p=0.29$; Supp. Fig. 8D). These data indicate that similar to Mrx6-Pet20, Mrx6-Pim1 colocalization also occurs in areas close to mtDNA. Taken together, our data suggest a hierarchy of assembly in which the Mrx6 complexes preferentially colocalize with mtDNA, whereas the individual components —or yet to be defined partially assembled subcomplexes— are mostly found in the areas devoid of mtDNA (Fig. 10).

Discussion

In this study we determined cellular components that modulate mtDNA levels in yeast using a forward genetic screen. We comprehensively determined mtDNA levels in the ~5100 mutants of a yeast deletion library and found that ~2% of these mutants had elevated levels of mtDNA compared to WT. Remarkably, the vast majority of these mutants (~85%) displayed less than a 2.5-fold increase in mtDNA levels, suggesting that a single gene deletion is not sufficient to drastically alter mtDNA levels. This finding suggests that mtDNA copy number is under stringent regulation, which may be explained by a multi-layered system involving a combination of various components such as factors regulating mtDNA replication and/or stability. One such layer that affects mtDNA levels is clearly cell size, as the majority of our hits with increased mtDNA copy number displayed increased cell size. This finding supports the notion that mtDNA copy number scales proportionally to mitochondrial network length, which in turn scales with cell volume (Osman et al., 2015; Rafelski et al., 2012). Therefore, in contrast to the nuclear genome, mtDNA copy number appears not to be determined on a 'per cell' basis, but rather on a 'per cell volume' basis. The molecular mechanisms underlying how mtDNA levels coordinate with mitochondrial volume remain a challenge.

Mrx6 is a regulator of mtDNA levels

Of the nine mutants that displayed elevated mtDNA levels and unaltered cell size, we examined the role of Mrx6 in maintenance of mtDNA levels. Our screen identified several other proteins such as Yor114w, Sam37, Ccs1, Rad27, Oar1, Sod1 and Mog1 that have been assigned with high-confidence as members mitochondrial proteome (Morgenstern et al., 2017). Of those, Aim4 and Mdm20 are involved in mitochondrial inheritance (Hermann et al., 1997; Hess et al., 2009). However, no common structural elements between Mrx6 and the other hits are apparent.

Mrx6 has been previously identified in a complex with the mitochondrial ribosome and named "Mitochondria oRganization of gene eXpression 6" (Kehrein et al., 2015). However to date, the function of Mrx6 has remained obscure. Based on the following observations, Mrx6 appears directly linked to mtDNA copy number regulation: 1) Δ*mrx6* cells do not display a growth defect on a non-fermentable carbon source, ruling out that mtDNA levels are elevated due to a compensatory feedback loop that responds to a defective respiratory chain, 2) Δ*mrx6* cells respond to a change in carbon source and display elevated mtDNA levels compared to WT on both fermentable and non-fermentable carbon sources, excluding the possibility that Δ*mrx6* cells are defective in glucose repression (Ulery et al., 1994); 3) Δ*mrx6* cells do not exhibit any changes in mitochondrial network length or morphology, which excludes that elevated mtDNA levels are caused by compromised mitochondrial structure. Thus, elevated mtDNA levels in Δ*mrx6* cells are not simply secondary effects caused by mitochondrial or cellular dysfunction.

Interestingly, deletion of *MRX6* results in elongated nucleoids. One plausible explanation for this phenotype is that newly replicated copies of mtDNA in Δ*mrx6* cells often remain associated with parental mtDNA, resulting in bigger and misshapen nucleoids. The oblong shape of nucleoids is reminiscent of halted DNA segregation, which could affect mtDNA levels. Alternatively, deletion of *MRX6* could change packaging of nucleoids, resulting in less compact and elongated nucleoids, which could alter mtDNA levels, perhaps by providing more access to origin of replication regions.

Mrx6 forms a complex with Pim1 and Pet20

Mrx6 contains a PET20-domain of uncharacterized structure and function that is conserved in fungi including distant species, such as *S. pombe*. Like Mrx6, Pet20 and Sue1 are the two other proteins in *S. cerevisiae* that carry PET20-domain, and they all are localized to mitochondria (Polevoda et al., 2006; Wei and Sherman, 2004). In contrast to *MRX6*, however, deletion of *PET20* or *SUE1*, alone or in combination, do not affect mtDNA levels suggesting that expression of PET20 domains in other molecular contexts is insufficient to compensate for Mrx6's specialized function.

Intriguingly, our mass spectrometry analyses revealed an exciting link between all three members of the PET20-domain protein family and the mitochondrial protein quality control system by placing all three PET20-domain proteins into an interaction network with the mitochondrial Lon protease, Pim1. The finding that co-purification of Pim1 with Pet20 depends on Mrx6 and that Mrx6 co-purifies with Pet20 suggests that Pim1, Mrx6 and Pet20 may be part of the same complex, whereas Sue1 forms an alternate complex with Pim1.

Mrx6's other interaction partner, Mam33, is a specific translational activator of Cox1 mRNA (Roloff and Henry, 2015). Moreover, Pim1-mediated proteolysis is necessary for processing and translation of mature Cox1 mRNA (van Dyck et al., 1998). While the physiological role of the interaction between Pim1, Mam33 and the PET20-domain proteins is currently not clear, an exciting possibility is that these proteins are functional adaptors that regulate the activity and/or determine the substrate specificity of Pim1. In agreement with such a role, Sue1 is required for degradation of labile forms of cytochrome c (Wei and Sherman, 2004), suggesting that Sue1-Pim1 dependent proteolysis could play a role for degradation of altered forms of cytochrome c (albeit it remains a paradox how misfolded cytochrome c would venture into the mitochondrial matrix space to meet its fate). By analogy, Mrx6 may be important for Pim1-dependent degradation of proteins regulating mtDNA copy number.

Lon proteases regulate mtDNA levels

Importantly, Pim1 has been previously linked to mtDNA biology. It colocalizes with nucleoids (Kunova et al., 2017), and its human homolog binds to mtDNA, preferentially in the control region where mtDNA transcription and replication are initiated (Lu et al., 2007).

Abf2, one of the substrates of Pim1, is a mitochondrial packaging protein that is required for stability of mtDNA (Bayot et al., 2010), and changes in expression level of Abf2 alter mtDNA copy number accordingly (Zelenaya-Troitskaya et al., 1998). The ortholog of Abf2 in higher eukaryotes, TFAM, also modulates mtDNA levels (Ekstrand et al., 2004; Kanki et al., 2004), and changes in Lon protease expression alter mtDNA copy number through degradation of TFAM (Lu et al., 2013; Matsushima et al., 2010). Taken together, these findings suggest a role for Lon proteases in regulation of mtDNA levels through Abf2/TFAM. In our hands, however, Abf2 protein levels did not change in Δ*mrx6* cells with respect to WT cells, suggesting that the increased mtDNA phenotype in Δ*mrx6* cells is not exerted by modulating Abf2 levels.

Hsp60, which is another substrate of Pim1, is a mitochondrial chaperone that binds to mtDNA at regions containing the origin of replication (Bayot et al., 2010; Kaufman et al., 2000). Cells having a temperature sensitive mutant of Hsp60 show an elongated nucleoid phenotype similar to what we observed in our study (Kaufman et al., 2003). Moreover, the mutant cells have defects in transmission of mtDNA to daughters, resulting accumulation of mtDNA in mother cells. By contrast to this earlier work, we did not detect any kind of mtDNA transmission defect in Δ*mrx6* cells. Taken together, these observations combined with our work indicate that molecular players leading mtDNA increase in Δ*mrx6* cells are different than these reported Pim1 substrates. Furthermore, the human mitochondrial Lon protease degrades mtDNA helicase, Twinkle, *in vitro* (Kunova et al., 2017), which is one of the limiting factors of mtDNA copy number (Tyynismaa et al., 2004). Given that the spectrum of Lon protease substrates is so large, a candidate approach for uncovering a causal link with mtDNA copy number control may be of limiting value.

Mitochondria are thought to have evolved as endosymbionts from ancestral bacteria. In this light, it is exciting that Lon proteases are also involved in regulating replication of bacterial genomes. *C. crescentus* and *E.coli* Lon proteases, for example, affect DNA replication by degrading a replication initiation factor and a inhibitor, respectively (Jonas et al., 2013; Langklotz and Narberhaus, 2011). Since we show that the Mrx6 complex identified here preferentially colocalizes with mtDNA, we can speculate that, by analogy to the bacterial DNA replication, the Mrx6 complex may serve bring Pim1 into a molecular context on mtDNA, acting as an adaptor/anti-adaptor for selective degradation of Pim1 substrates that in turn control mtDNA levels, perhaps by regulating mtDNA replication. Further characterization of Pim1-Mrx6-Pet20-Mam33 complex and its interaction with mtDNA will be important to understand the mechanism(s) by which Mrx6 affects mtDNA copy number control and how this process has been modified in evolution.

Material and Methods

Yeast strains and plasmids

Yeast strains used in this study are derived from W303 and are listed in Table S2. Deletion of yeast genes was performed in diploid strains and C' terminal tagging of genes was done in haploid strains using homologous recombination as described previously (Janke et al., 2004). Haploid cells were used for all experiments, except those shown in Figs. 2A, 3 and 4 where diploids cells were used. Plasmids and oligonucleotides used in this study are listed in Table S3 and Table S4, respectively.

Colony blot hybridization

A previously described protocol (Kleinman, 1996) was followed with some additional steps to optimize the protocol for fluorescent hybridization. Briefly, the mutants of the yeast deletion library were grown on glucose rich agar plates and transferred to nylon membranes (Bright Star-plus was used for the 1st and 2nd screens and Pall Biodyne A was used for the 3rd screen) by incubating membranes on plates for 5 min followed by gentle lifting. Membranes were air dried for 5 min and placed, colony side up, on Whatman 3M papers that were soaked with reducing buffer (1M Sorbitol, 50 mM DTT, 20 mM EDTA, 10 mM NaAzide, 10 mM KF) and kept at RT for 20 min. Subsequently, membranes were transferred onto Whatman 3M papers that were soaked with lysis buffer (1 M Sorbitol, 10 mM DTT, 20 mM EDTA, 10 mM Tris-HCl pH=7.6, 10 mM NaAzide, 10 mM KF, 3mg/ml Zymolase 20-T) and kept at 37°C in a closed container overnight. The next day, membranes were placed on Whatman 3M papers that were soaked with 0.5 M NaOH for 10 min. Membranes were air dried for 5 min and neutralized by incubating on Whatman 3M papers saturated with 0.5 M Tris-HCl pH=7.5/ 5X SSC for 5 min, 2 times, and transferred onto Whatman 3M papers saturated with TE pH=7.5 / 1X SSC (150mM NaCl, 15mM sodium citrate) for 5 min. Following neutralization, membranes were placed on Whatman 3M papers soaked with TE pH=7.5 / 1X SSC buffer with 0.2 mg/ml RNaseA (Sigma) and kept in a closed container for 2 hours at 37°C. Subsequently, membranes were placed on 3M Whatman papers that were soaked with 100 mM Tris-HCl pH=7.5 / 1X SSC for 5 min for 2 times, air dried and baked at 65°C for 30 min, followed by UV-crosslinking at 60 mJ/cm^2 with 254 nm irradiation. Membranes were placed into hybridization bottles and washed 2 times with 5X SSC, 0.5% SDS, 10 mM EDTA for 15 min while rotating at 65°C. Membranes were rinsed with Proteinase K buffer (50mM Tris HCl pH=7.5, 10 mM EDTA, 1% SDS, 50 mM NaCl) and incubated in Proteinase K buffer containing 2 mg/ml Proteinase K (Invitrogen) for 2 h at 55°C. Membranes were rinsed with 5X SSC and washed with 3M Urea, 1% SDS at 55°C, 3 times for 10 min each. Membranes were further washed with 5X SSC 2 times for 15 min each and pre-hybridized for 2 hours with hybridization buffer (50% Formamide, 8% Dextran Sulfate, 2.5X SSC, 5 mM EDTA, 25 mM Hepes-KOH pH=7, 3% SDS) at 42°C. Membranes were hybridized with fluorescently labeled probes (final concentration 100ng/ml of mtDNA-Cy3 probe mix and 100ng/ml nuclear DNA-Cy5 probe mix) in hybridization buffer at 42°C overnight. The next day, membranes were washed with wash buffer (1X SSC, 1% SDS) 3 times for 10 min each at 65°C. Membranes were completely air dried prior to scanning with a Typhoon Fluorescent Scanner using Cy3 and Cy5 channels in normal sensitivity.

Preparation of probes for hybridization

Probes were prepared by PCR using Phusion DNA Polymerase and different pairs of primers (Table S4). 12 different probes were pooled to detect nuclear DNA and 2 different probes were pooled to detect mtDNA. PCR products were cleaned-up and concentrated with Zymo DNA Clean & Concentrator-5 and labeled with Mirus *Label* IT Nucleic Acid Labeling Kits using Cy3 or Cy5 dyes overnight according to the product manual. Labeled probes were EtOH precipitated and stored at -30°C. Probes were boiled for 5 mins before addition into hybridization buffer.

Quantification of colony blots

Scans of colony blots were quantified with ImageJ. The median signal intensity of each colony, for Cy3 and Cy5 channels, was determined after background subtraction by using a rolling ball plugin. Auto-fluorescence of yeast colonies was measured in both channels from a sample membrane that had not been incubated with probes. Auto-fluorescence of colonies linearly correlated with colony size, and thus we developed an algorithm that calculates auto-fluorescence for each mutant depending on its colony size. The hybridization signal for each colony was calculated by subtracting the estimated auto-fluorescence from the median signal intensity. However, later we found out that auto-fluorescence also correlates with respiratory capability, which explains why the mutants that lack mtDNA have mtDNA/nDNA ratios below zero after subtraction of colony auto-fluorescence. To calculate relative fold changes in mtDNA/nDNA ratios, mtDNA/nDNA ratios of all mutants except the ones that had lost mtDNA were averaged and used for normalization of each mutant mtDNA/nDNA ratio.

Cell growth and quantitative PCR

Prior to harvesting, yeast cells were grown in liquid media (YPD, YPEG or drop-out synthetic media) in log-phase for 24 hours at 30°C. In Fig. 2C, cells were treated with 0.5mM H_2O_2 in YPD for 1 hour. In Fig. 2D, cells were treated with DMSO or FCCP (5ug/ml) in YPD for 1 hour. Genomic DNA (gDNA) was extracted using the Thermo Scientific Pierce Yeast DNA Extraction Reagent or Zymo ZR-96 Fungal/Bacterial DNA kits. gDNA was subjected to qPCR using iQ- Syber Green Supermix (Bio-RAD) and primers specific for Cox1 and Act1 genes according to the manufacturer's manual (Table S4). For absolute mtDNA copy number quantification, 1kb fragments of Cox1 and Act1 genes were cloned into pUC19 plasmids and used as standards for copy number quantification. For statistical analysis of qPCR data, unpaired t test was used for comparison of two groups and one-way ANOVA was used for multiple comparisons, followed by Tukey's multiple comparison test in GraphPad Prism.

Flow cytometry

Yeast cells were grown in liquid media (YPD) in 96-well polystyrene plates overnight at 30°C, and the next morning diluted, regrown for ~4 doubling times and harvested at $O.D._{600}$=~0.5-1. Yeast cultures were then transferred to 96-well microplates (Corning), diluted with YPD one to five ratio and analyzed by a flow cytometer (LSR II, Beckton-Dickinson), and a high throughput sampler (BD High Throughput Sampler, Beckton-Dickinson) to inject samples into the flow cytometer. The SSC-H parameter was used as an estimate of cell size and the SSC-H values of the mutants were normalized to the value of WT. Cell size of some mutants was also analyzed by microscopy to verify cell size increase. The remaining cultures were used for gDNA isolation and subjected to qPCR for mtDNA analysis for Fig. 1D.

Growth analysis

Yeast cells were grown in liquid media (YPD) in log-phase for 24 hours at 30°C and diluted to O.D.$_{600}$ =0.05 in total 100 µl YPD or diluted to O.D.$_{600}$ =0.1 in total 100 µl YPEG in a 96-well clear bottom microplate (Corning). The wells on the edges of the plate were filled with YPD to maintain humidity and the lid was secured by using a tape that partially covered the plate to allow air exchange. Growth assays were conducted at 30°C by using Tecan Infinite 200 Pro plate reader for 48 hours with a kinetic interval of 15 min.

Immunoprecipitation

Immunoprecipitations were performed as previously described (Friedman et al., 2015). Briefly, 500 OD_{600} cells grown in log-phase in YPD at 30°C, were harvested by centrifugation, resuspended in 5 ml of lysis buffer (20 mM HEPES pH=7.4, 150 mM KOAc, 2 mM $Mg(OAc)_2$, 1 mM EGTA, 0.6 M sorbitol), and protease inhibitor cocktail was added to 1x (EDTA free, Roche). Cell suspension was flash-frozen dropwise in liquid N_2, and lysed using a ball mill (Retsch MM301). The cell powder was thawed in RT, and unbroken cells and large debris were pelleted using GH-3.8 rotor at 1500 rpm for 5 min at 4°C. For solubilization, digitonin was added to the supernatant to a final concentration of 1%. Samples were incubated for 30 min at 4°C, and cleared by centrifugating at 12,000 x g at 4°C. 50 µl µMACS anti-Flag beads (Miltenyi Biotec) were added to the supernatant and incubated 45 min at 4°C, followed by isolation with µ columns and a µMACS separator (Miltenyi Biotec). Columns were washed 3 times with lysis buffer, 0.1% digitonin and 1x protease inhibitor, and 2 times with only lysis buffer. Samples were eluted using on-bead trypsin digest by incubating beads with 25 µl of elution buffer I (2M Urea, 50 mM Tris-HCl pH=7.5, 1mM DTT and 5 µg/ml trypsin (Trypsin Gold, Promega)) for 30 min at RT. 50 μl of elution buffer II (2M Urea, 50 mM Tris-HCl, pH=7.5, 5 mM chloroacetamide) was added to the column, 2 times, to collect elutions. Elutions were kept at RT overnight to continue digestion. Mass spectrometric proteomic analysis was performed at the Genome Center Proteomics Core of the University of California, Davis.

Western Blot analysis

For Fig. 7A, the samples eluted from the μMACS beads by incubating beads with preheated (95°C) 1x SDS loading buffer instead of trypsin digestion. For Figs. 2A and Supp. 8, proteins were extracted from 1 $O.D._{600}$ cells in Urea-CHAPS buffer (20mM Tris-HCl pH=7.4, 7 M Urea, 2 M thiourea, 4% CHAPS) by 3 min bead beating at 4°C. Protein concentration of each sample was measured by Pierce BCA protein assay kit (Thermo Scientific). Samples were boiled for 5 min in SDS loading dye and BME prior to SDS-PAGE analysis, transferred to nitrocellulose membrane, and immuno-blotted with the following primary antibodies at the indicated concentrations in 5% milk PBS-T buffer: mouse anti-FLAG M2 (1:5000, Sigma–Aldrich); rabbit anti-Pim1 (1:1000, kindly provided by C. Suzuki); mouse anti-myc 9E10 (1:1000, Santa Cruz); mouse anti-PGK1 (1:5000, abcam); rabbit anti-Tom40 (1:30000, kindly provided by T. Langer); rabbit anti-Abf2 (1:1000, kindly provided by J. Nunnari).

SI microscopy and analysis

For Fig. 3A, slides were prepared as previously described (Kaplan and Ewers, 2015). Briefly, microscope coverslips (High Precision) were cleaned with a plasma cleaner (PDC-001, Harrick Plasma) and treated with Concanavalin A (Sigma; 5mg/ml) for 30 min, spin-coated for 15 sec and air-dried for 15 min in a vacuum desiccator. Prior to imaging, yeast cells were grown in liquid drop-out synthetic media in log-phase for 24 hours at 30°C. 0.5 $O.D._{600}$ cells were spun down, washed and resuspended in 100 µl PBS. 20 µl cell suspension was added on the Concanavalin A treated coverslips and incubated for 15 min. Unattached cells were washed with PBS. For fixation, cells were incubated twice for 5 min with 4% paraformaldehyde (Electron Microscopy Sciences) in PBS on coverslips. Fixation was followed by quenching with 50 mM NH_4Cl, 2 times, 10 min each. Cells were washed with PBS and a drop of anti-fade media (Vectashield) was added before mounting coverslips to slides. Slides were imaged using DeltaVision OMX SR (GE) using SIM mode and a 60x/1.42 NA oil objective. The Imaris software was used to detect/count LacI-GFP foci and to segment the mitochondrial network in three dimensions. Quantification of mitochondrial network length, mitochondrial endpoints and distribution of mtDNA was performed as described previously (Osman et al., 2015). Three- or four-way junctions of the segmented mitochondrial network were scored as branchpoints.

For Fig. 4A, yeast cells were grown in liquid drop-out synthetic media in log-phase for 24 h at 30°C and fixed with 4% Paraformaldehyde (Electron Microscopy Sciences) in growth media for 30 min at RT. Cells were prepared as described previously (Silver, 2009). Briefly, cells were pelleted and washed 2 times with P solution (0.1M $KHPO_4$, 1.2M Sorbitol) and resuspended in 1 ml of P solution. 15 µl of 10 mg/ml Zymolase (T-20) and 5 µl BME were added to the solution, and incubated at RT for 30 min. Cells were gently washed with P solution once and resuspended in 0.5 ml of P solution. Microscope coverslips (High Precision) were plasma cleaned and coated with 0.1% poly-L-lysine for 20 min. Coverslips were washed 2 times with ddH_2O and air dried completely. 30 µl of cell suspension was added and incubated 20 min. Excess media were aspirated and coverslips were plunged into ice-cold methanol for 6 mins, followed by submerging into ice-cold acetone for 30 sec. Coverslips were air dried briefly and incubated with 3% BSA (Sigma) in PBS for 1 h at RT. Cells were stained with DAPI (Invitrogen; 5 μg/ml) for 5 min and washed 2 times with PBS. Coverslips were mounted to slides after addition of a drop of anti-fade medium (Vectashield). Slides were imaged using DeltaVision OMX SR (GE) using SIM mode and a 60x/1.42 NA oil objective. The Imaris software was used to calculate the number of DAPI stained-nucleoids and the volume of each nucleoid in three dimensions.

Immunofluorescence and analysis

Cells were prepared for immunofluorescence as it was done before for the cells shown in Fig. 4A, except after acetone treatment cells were incubated with blocking buffer, 3% Goat Serum (Jackson ImmunoResearch) in PBS for 1 h at RT, followed by incubation with mouse anti-DNA antibody (1:1000, abcam) in blocking buffer overnight at 4°C. The next day, cells were washed 3 times with blocking buffer and incubated with anti-mouse secondary antibody conjugated with Alexa Fluor 405 (1:500) or Alexa Fluor 647 (1:1000) for an hour and a half at RT at dark. Subsequently, cells were washed 3 times with blocking buffer and 2 times with PBS, and if necessary stained with DAPI (5μg/ml) for 5 min and washed 2 times with PBS. Coverslips were mounted to slides after addition of a drop of anti-fade medium (Vectashield). Slides were imaged using DeltaVision OMX SR (GE) using conventional mode and a 60x/1.42 NA oil objective. Deconvolution of images and maximum projection of Z stacks done by using DeltaVision SoftWorRx. Quantification of nucleoid length was performed as follows. First, a curved line was manually drawn through the mitochondrial network of each cell and the line's one-dimensional intensity profile was extracted. Then, nucleoids were automatically picked out from the intensity profile by adaptive thresholding. Local threshold values were individually calculated for each data point using Li's minimum cross entropy method applied within a 4.8 μm long sliding window (Li, 1993). The sliding window approach allowed us to compensate for nonuniform fluorescent background in the images and to robustly identify peaks in the intensity profile in an unbiased way (Supp. Fig. 3A). We carried out our experiments to determine the length of nucleoids using both conventional and super-resolution (structured illumination) microscopy (Fig. 4) and found that the increase in nucleoid length in Δ*mrx6* cells is robustly detected by both methods.

Live microscopy and analysis

Microscope coverslips (High Precision) were plasma cleaned and treated with Concanavalin A (0.5 mg/ml) for 15 min, spin-coated for 15 sec and air-dried for 15 min in a vacuum desiccator. Prior to imaging, yeast cells were grown in liquid drop-out synthetic media in log-phase for 24 h. DAPI was added to media (1 μg/ml final concentration) for 15 min if needed. 0.5 $O.D._{600}$ cells were spun down, washed and resuspended in 20 μl drop-out synthetic media lacking sugar. Cell suspension was added on the concanavalin A-treated cover slips and incubated for 5 min. Unattached cells were washed with drop-out synthetic media. Slides were imaged using DeltaVision OMX SR (GE) using conventional mode and a 60x/1.42 NA oil objective. Deconvolution of images and maximum projection of Z stacks done by using DeltaVision SoftWorRx. Intensity profiles were obtained with ImageJ by measuring pixel intensities along mitochondrial tubules of Z-projected images using the line draw tool (settings: line width=3). Intensity profiles along identical lines from different channels were used to calculate the Pearson's Correlation Coefficients (PCC) (Supp. Fig. 5C). The Manders' Colocalization Coefficients (MCC) were calculated after thresholding intensity profiles using

Yen's method (Yen et al., 1995). To assess significance of colocalizations, MCC and PCC were determined for intensity profiles of two channels, of which one intensity profile was randomized by scrambling blocks of 5 values (400 nm) in the line profiles. Scrambling blocks of values rather than single values has been shown to give a more accurate probability distribution, because it retains autocorrelation between neighboring pixels (Costes et al., 2004). Statistical significance of PCC and MCC values between measured and randomized intensity profiles was determined by applying the independent t-test.

To test whether fractions of Mrx6 or Pet20 that colocalize with Pim1 preferentially colocalize with DAPI, intensity profiles for Mrx6-Neon or Pet20-Neon and Pim1-Ruby were first thresholded with Yen's method and then multiplied with one another. Values greater then 0 in the resulting profile were scored as colocalizing fractions, whereas values equal to 0 were scored as non-colocalizing fractions. MCC values between colocalizing or non-colocalizing fractions of Mrx6-Neon-Pim1-Ruby or Pet20-Neon-Pim1-Ruby and DAPI were determined as described in the previous paragraph. To assess significance of this analysis, the same analysis was performed with a randomized DAPI profile. A t-test was used to infer statistical significance between MCC values determined for the real data and the randomized data.

Acknowledgments

We thank to Jodi Nunnari, David Morgan, Wallace Marshall, Patrick O'Farrell and members of the Walter lab for their technical advice and insightful discussions. We thank to Carolyn Suzuki for providing the anti-Pim1 antibody, Jodi Nunnari for the anti-Abf2 antibody and Thomas Langer for the anti-Tom40 antibody, Voytek Okreglak, Hansong Ma, Jeiwei Xu, Jason Wojcechowskyj, Ingacio Zuleta, Ricardo Almeida, Amy Chang, Shoshana Brown, Samantha Lewis, Justin M. Yamada for reagents, technical advice and their helpful discussions, Anne Pipathsouk and Roberto Diaz for their technical help during their rotation and internship, respectively. We also thank Nikon Imaging Center at UCSF and Proteomics Core Facility at UC Davis for their invaluable contributions. This work was supported by a UCSF Zaffaroni Fellowship (to AG) and Howard Hughes Medical Institute (HHMI) International Student Research Fellowships (to AG and AM). VB is a Damon Runyon Fellow supported by the Damon Runyon Cancer Research Foundation (DRG-2284-17). CO was funded by the Simons Foundation (# 326844). PW is a HHMI Investigator.

References

Bayot, A., M. Gareil, A. Rogowska-Wrzesinska, P. Roepstorff, B. Friguet, and A.L. Bulteau. 2010. Identification of novel oxidized protein substrates and physiological partners of the mitochondrial ATP-dependent Lon-like protease Pim1. *J Biol Chem*. 285:11445-11457.

Chen, X.J., and R.A. Butow. 2005. The organization and inheritance of the mitochondrial genome. *Nat Rev Genet*. 6:815-825.

Connelly, C.F., and J.M. Akey. 2012. On the prospects of whole-genome association mapping in Saccharomyces cerevisiae. *Genetics*. 191:1345-1353.

Conrad, M.N., and C.S. Newlon. 1982. The regulation of mitochondrial DNA levels in Saccharomyces cerevisiae. *Curr Genet*. 6:147-152.

Costes, S.V., D. Daelemans, E.H. Cho, Z. Dobbin, G. Pavlakis, and S. Lockett. 2004. Automatic and quantitative measurement of protein-protein colocalization in live cells. *Biophys J*. 86:3993-4003.

Ekstrand, M.I., M. Falkenberg, A. Rantanen, C.B. Park, M. Gaspari, K. Hultenby, P. Rustin, C.M. Gustafsson, and N.G. Larsson. 2004. Mitochondrial transcription factor A regulates mtDNA copy number in mammals. *Hum Mol Genet*. 13:935-944.

Friedman, J.R., A. Mourier, J. Yamada, J.M. McCaffery, and J. Nunnari. 2015. MICOS coordinates with respiratory complexes and lipids to establish mitochondrial inner membrane architecture. *eLife*. 4:e07739.

Hermann, G.J., E.J. King, and J.M. Shaw. 1997. The yeast gene, MDM20, is necessary for mitochondrial inheritance and organization of the actin cytoskeleton. *J Cell Biol*. 137:141-153.

Hess, D.C., C.L. Myers, C. Huttenhower, M.A. Hibbs, A.P. Hayes, J. Paw, J.J. Clore, R.M. Mendoza, B.S. Luis, C. Nislow, G. Giaever, M. Costanzo, O.G. Troyanskaya, and A.A. Caudy. 2009. Computationally driven, quantitative experiments discover genes required for mitochondrial biogenesis. *PLoS Genet*. 5:e1000407.

Janke, C., M.M. Magiera, N. Rathfelder, C. Taxis, S. Reber, H. Maekawa, A. Moreno-Borchart, G. Doenges, E. Schwob, E. Schiebel, and M. Knop. 2004. A versatile toolbox for PCR-based tagging of yeast genes: new fluorescent proteins, more markers and promoter substitution cassettes. *Yeast*. 21:947-962.

Jonas, K., J. Liu, P. Chien, and M.T. Laub. 2013. Proteotoxic stress induces a cell-cycle arrest by stimulating Lon to degrade the replication initiator DnaA. *Cell*. 154:623-636.

Kanki, T., K. Ohgaki, M. Gaspari, C.M. Gustafsson, A. Fukuoh, N. Sasaki, N. Hamasaki, and D. Kang. 2004. Architectural role of mitochondrial transcription factor A in maintenance of human mitochondrial DNA. *Mol Cell Biol*. 24:9823-9834.

Kaplan, C., and H. Ewers. 2015. Optimized sample preparation for single-molecule localization-based superresolution microscopy in yeast. *Nat Protoc*. 10:1007-1021.

Kaufman, B.A., J.E. Kolesar, P.S. Perlman, and R.A. Butow. 2003. A function for the mitochondrial chaperonin Hsp60 in the structure and transmission of mitochondrial DNA nucleoids in Saccharomyces cerevisiae. *J Cell Biol*. 163:457-461.

Kaufman, B.A., S.M. Newman, R.L. Hallberg, C.A. Slaughter, P.S. Perlman, and R.A. Butow. 2000. In organello formaldehyde crosslinking of proteins to mtDNA: identification of bifunctional proteins. *Proc Natl Acad Sci U S A*. 97:7772-7777.

Kehrein, K., R. Schilling, B.V. Moller-Hergt, C.A. Wurm, S. Jakobs, T. Lamkemeyer, T. Langer, and M. Ott. 2015. Organization of Mitochondrial Gene Expression in Two Distinct Ribosome-Containing Assemblies. *Cell Rep*. 10:843-853.

Kleinman, M.J. 1996. Yeast colony hybridization. *Methods Mol Biol*. 53:189-192.

Kunova, N., G. Ondrovicova, J.A. Bauer, J. Bellova, L. Ambro, L. Martinakova, V. Kotrasova, E. Kutejova, and V. Pevala. 2017. The role of Lon-mediated proteolysis in the dynamics of mitochondrial nucleic acid-protein complexes. *Sci Rep*. 7:631.

Langklotz, S., and F. Narberhaus. 2011. The Escherichia coli replication inhibitor CspD is subject to growth-regulated degradation by the Lon protease. *Mol Microbiol*. 80:1313-1325.

Li, C.H., and C.K. Lee. 1993. Minimum Cross Entropy Thresholding. *Pattern Recognition*. 26:617-625.

Lu, B., J. Lee, X. Nie, M. Li, Y.I. Morozov, S. Venkatesh, D.F. Bogenhagen, D. Temiakov, and C.K. Suzuki. 2013. Phosphorylation of human TFAM in mitochondria impairs DNA binding and promotes degradation by the AAA+ Lon protease. *Mol Cell*. 49:121-132.

Lu, B., S. Yadav, P.G. Shah, T. Liu, B. Tian, S. Pukszta, N. Villaluna, E. Kutejova, C.S. Newlon, J.H. Santos, and C.K. Suzuki. 2007. Roles for the human ATP-dependent Lon protease in mitochondrial DNA maintenance. *J Biol Chem*. 282:17363-17374.

MacAlpine, D.M., P.S. Perlman, and R.A. Butow. 2000. The numbers of individual mitochondrial DNA molecules and mitochondrial DNA nucleoids in yeast are co-regulated by the general amino acid control pathway. *EMBO J*. 19:767-775.

Matsushima, Y., Y. Goto, and L.S. Kaguni. 2010. Mitochondrial Lon protease regulates mitochondrial DNA copy number and transcription by selective degradation of mitochondrial transcription factor A (TFAM). *Proc Natl Acad Sci U S A*. 107:18410-18415.

Meeusen, S., and J. Nunnari. 2003. Evidence for a two membrane-spanning autonomous mitochondrial DNA replisome. *J Cell Biol*. 163:503-510.

Morgenstern, M., S.B. Stiller, P. Lubbert, C.D. Peikert, S. Dannenmaier, F. Drepper, U. Weill, P. Hoss, R. Feuerstein, M. Gebert, M. Bohnert, M. van der Laan, M. Schuldiner, C. Schutze, S. Oeljeklaus, N. Pfanner, N. Wiedemann, and B. Warscheid. 2017. Definition of a High-Confidence Mitochondrial Proteome at Quantitative Scale. *Cell Rep*. 19:2836-2852.

Osman, C., T.R. Noriega, V. Okreglak, J.C. Fung, and P. Walter. 2015. Integrity of the yeast mitochondrial genome, but not its distribution and inheritance, relies on mitochondrial fission and fusion. *Proc Natl Acad Sci U S A*. 112:E947-956.

Polevoda, B., Y. Panciera, S.P. Brown, J. Wei, and F. Sherman. 2006. Phenotypes of yeast mutants lacking the mitochondrial protein Pet20p. *Yeast*. 23:127-139.

Rafelski, S.M., M.P. Viana, Y. Zhang, Y.H. Chan, K.S. Thorn, P. Yam, J.C. Fung, H. Li, F. Costa Lda, and W.F. Marshall. 2012. Mitochondrial network size scaling in budding yeast. *Science*. 338:822-824.

Roloff, G.A., and M.F. Henry. 2015. Mam33 promotes cytochrome c oxidase subunit I translation in Saccharomyces cerevisiae mitochondria. *Mol Biol Cell*. 26:2885-2894.

Silver, P. 2009. Indirect immunofluorescence labeling in the yeast Saccharomyces cerevisiae. *Cold Spring Harb Protoc*. 2009:pdb prot5317.

Taylor, S.D., H. Zhang, J.S. Eaton, M.S. Rodeheffer, M.A. Lebedeva, W. O'Rourke T, W. Siede, and G.S. Shadel. 2005. The conserved Mec1/Rad53 nuclear checkpoint pathway regulates mitochondrial DNA copy number in Saccharomyces cerevisiae. *Mol Biol Cell*. 16:3010-3018.

Traven, A., A. Janicke, P. Harrison, A. Swaminathan, T. Seemann, and T.H. Beilharz. 2012. Transcriptional profiling of a yeast colony provides new insight into the heterogeneity of multicellular fungal communities. *PLoS One*. 7:e46243.

Tyynismaa, H., H. Sembongi, M. Bokori-Brown, C. Granycome, N. Ashley, J. Poulton, A. Jalanko, J.N. Spelbrink, I.J. Holt, and A. Suomalainen. 2004. Twinkle helicase is essential for mtDNA maintenance and regulates mtDNA copy number. *Hum Mol Genet*. 13:3219-3227.

Ulery, T.L., S.H. Jang, and J.A. Jaehning. 1994. Glucose repression of yeast mitochondrial transcription: kinetics of derepression and role of nuclear genes. *Mol Cell Biol*. 14:1160-1170.

van Dyck, L., W. Neupert, and T. Langer. 1998. The ATP-dependent PIM1 protease is required for the expression of intron-containing genes in mitochondria. *Genes Dev*. 12:1515-1524.

Venkatesh, S., J. Lee, K. Singh, I. Lee, and C.K. Suzuki. 2012. Multitasking in the mitochondrion by the ATP-dependent Lon protease. *Biochim Biophys Acta*. 1823:56-66.

Wei, J., and F. Sherman. 2004. Sue1p is required for degradation of labile forms of altered cytochromes C in yeast mitochondria. *J Biol Chem*. 279:30449-30458.

Yen, J.C., F.J. Chang, and S. Chang. 1995. A new criterion for automatic multilevel thresholding. *IEEE Trans Image Process*. 4:370-378.

Zelenaya-Troitskaya, O., S.M. Newman, K. Okamoto, P.S. Perlman, and R.A. Butow. 1998. Functions of the high mobility group protein, Abf2p, in mitochondrial DNA segregation, recombination and copy number in Saccharomyces cerevisiae. *Genetics*. 148:1763-1776.

FIGURES AND TABLES

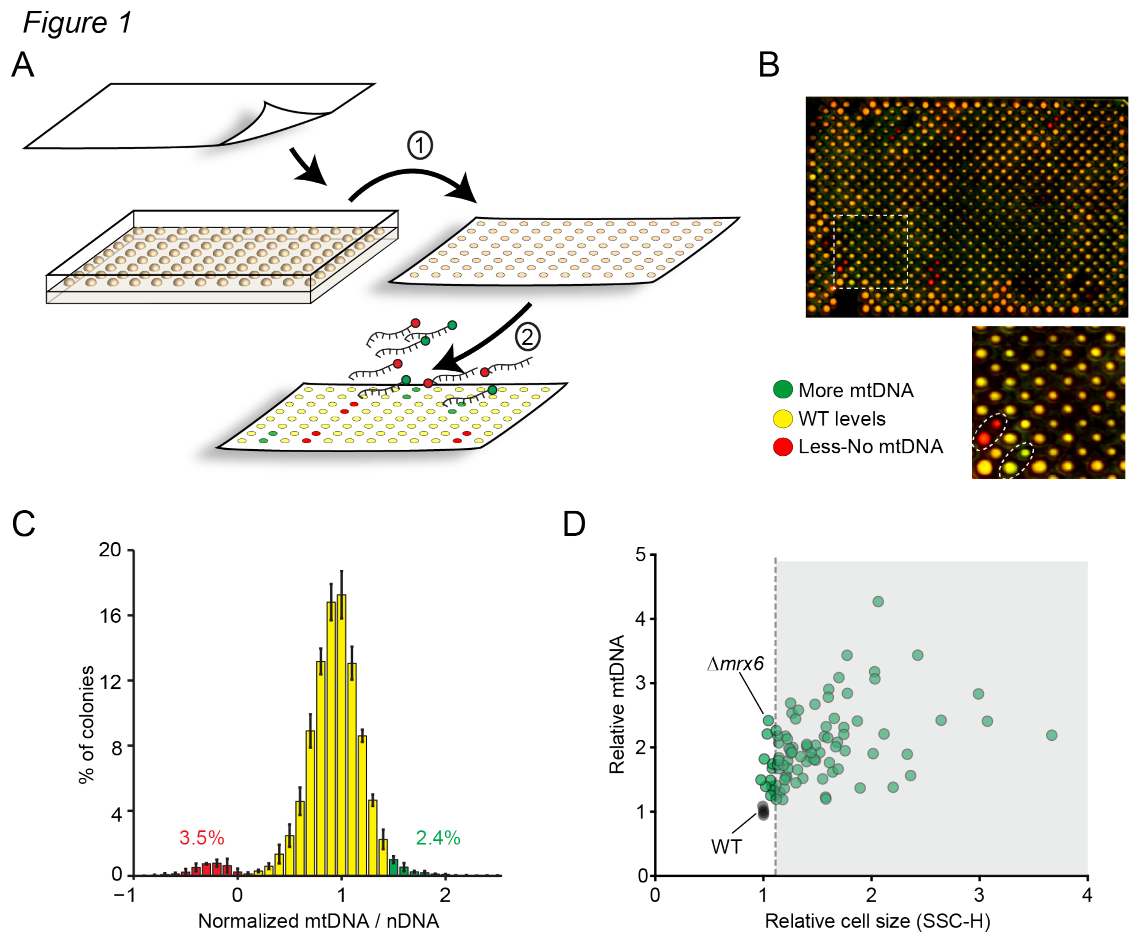

E

Gene ID	Gene name	Relative mtDNA (qPCR)	SEM (qPCR)	Relative cell size (SSC-H)	SEM (SSC-H)
YNL295W	*MRX6*	2.42	0.13	1.05	0.00
YOL076W	*MDM20*	2.26	0.22	1.12	0.07
YOR114W	*YOR114W*	2.21	0.39	1.03	0.01
YDR448W	*ADA2*	1.82	0.07	1.01	0.04
YLR176C	*RFX1*	1.74	0.06	1.09	0.01
YDL049C	*KNH1*	1.68	0.09	1.08	0.01
YGR252W	*GCN5*	1.50	0.08	0.98	0.07
YMR100W	*MUB1*	1.49	0.27	1.07	0.00
YBR194W	*AIM4*	1.39	0.09	1.02	0.01

Figure 1: A forward genetic screen to identify cellular machineries regulating mtDNA copy number

A) Schematic illustration of the genetic screen. Mutants of the yeast deletion library were grown on agar plates (fermentable rich media, YPD) and transferred to nylon membranes (1), lysed and hybridized with two sets of fluorescent probes specific for mitochondrial DNA (green) or nuclear DNA (red)(2).

B) Scan of a colony blot is shown as overlay of two channels. Each mutant has its replicate on the diagonal. Mutants with mtDNA/nDNA ratios similar to WT appear yellow; whereas mutants with increased or decreased mtDNA levels are depicted in green and red, respectively.
C) Histogram showing distribution of relative fold changes in mtDNA/nDNA ratios of the mutants. Error bars indicate standard deviations (SD) of three independent colony blot experiments (n=3). 2.4% of total mutants showed an increase in mtDNA copy number by at least 50% (green). 3.5% of total mutants lost the majority of or lack mtDNA (red). mtDNA/nDNA ratios below zero is due to subtraction of colony auto-fluorescence from hybridization signal (Supp. Fig. 1; for the list of mutants see Supp. Table 1).
D) mtDNA levels of 91 hits identified by colony blot screens, were verified by qPCR, shown as an average of two independent experiments. Cell sizes of mutants were determined by flow cytometry using SSC-H. Values are relative to WT (see Supp. Table 1.4). Three mutants showing budding defects were omitted from analysis; WT shown in black. Dashed line marks 10% cut off. Cells were grown in YPD.
E) The list of genes identified in this study; their deletion mutants lead to an increase in mtDNA copy number but their cell size remained within 10% change of WT. mtDNA levels and cell sizes were determined relative to WT (n=2).

Figure 2

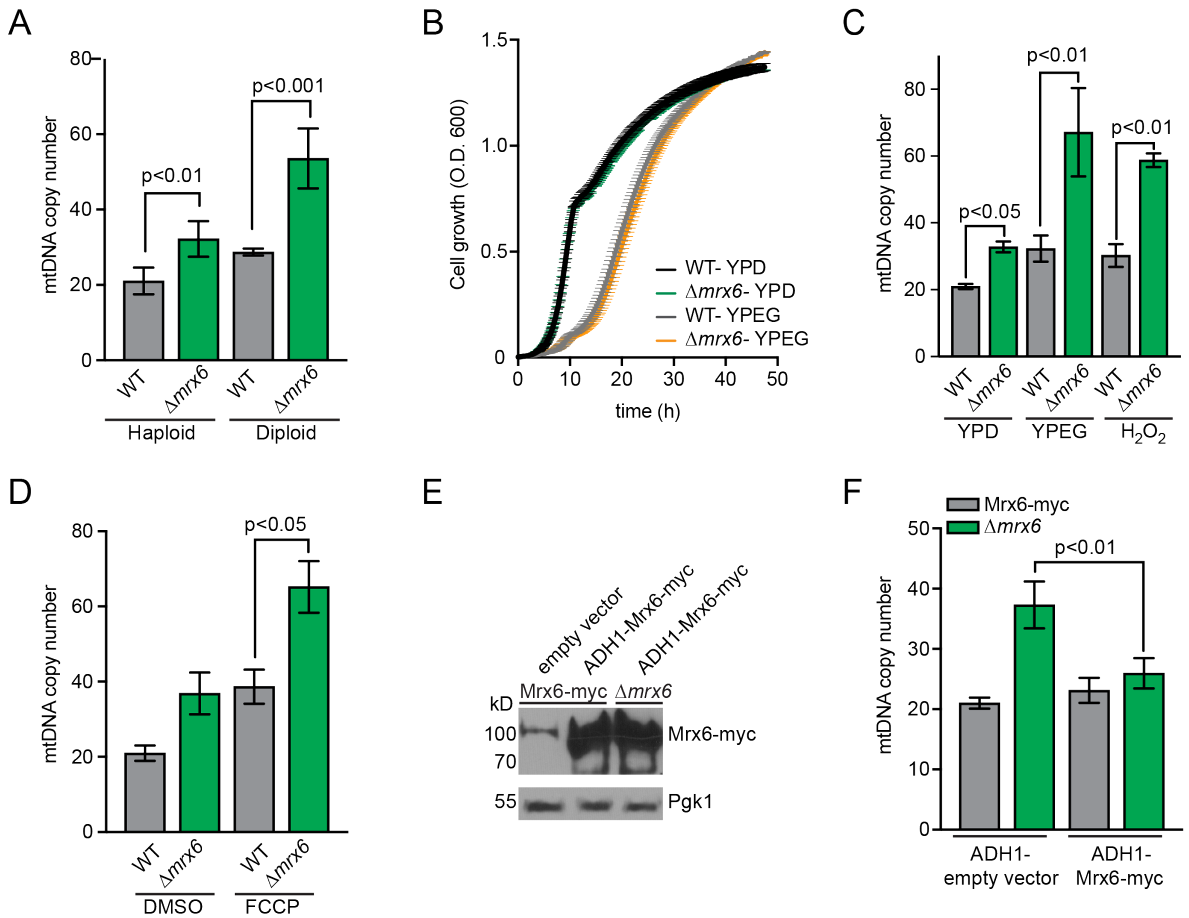

Figure 2: Deletion of an uncharacterized gene, *MRX6*, increases mtDNA copy number

A) qPCR analyses of mtDNA copy number in haploid and diploid W303 cells lacking *MRX6.* Cells were grown in YPD. Error bars indicate SD (n=4).
B) Growth curves of WT and Δ*mrx6* cells grown in YPD or YPEG (rich media with ethanol and glycerol). (n=2).
C) qPCR analyses of mtDNA levels in WT and Δ*mrx6* cells grown in YPD, YPEG or treated with 0.5mM H_2O_2 in YPD for one hour. (YPD and YPD+ H_2O_2, n=2; YPEG, n=4).
D) qPCR analyses of mtDNA levels in WT and Δ*mrx6* cells grown in YPD and treated with DMSO or FCCP (5μg/ml) for one hour. (n=2).
E) Western Blot analyses of Mrx6-myc levels in cells that either express Mrx6-myc or lack Mrx6, transformed with an empty vector or a vector allowing overexpression of Mrx6–myc from the ADH1 promoter. Cells were grown in drop-out synthetic media with dextrose, lacking URA (SD-ura). PGK1 was used as a loading control.
F) qPCR analysis of mtDNA copy number in cells over-expressing Mrx6–myc, shown in Fig. 2E. (n=4).

Figure 3

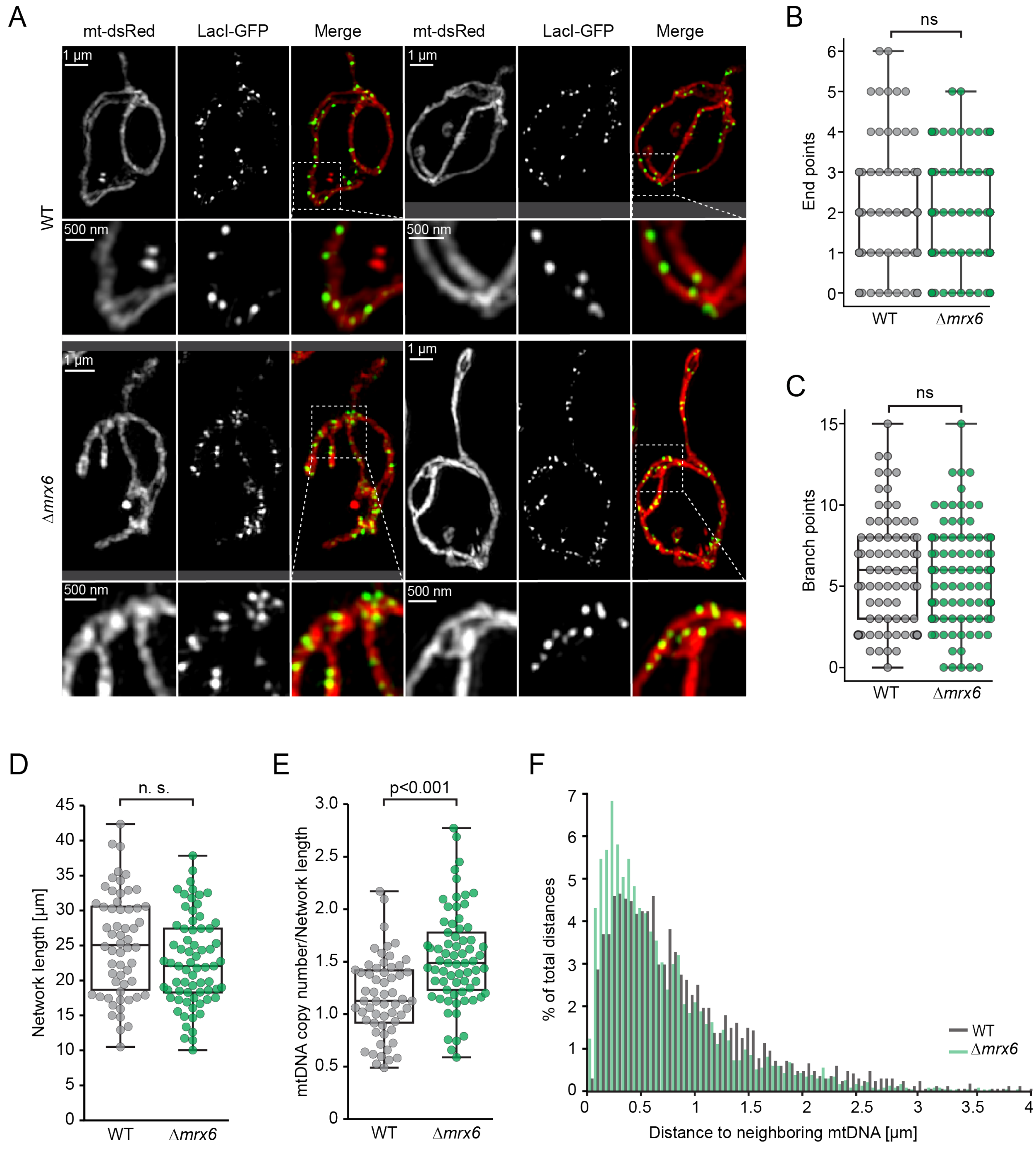

Figure 3: Deletion of *MRX6* increases mtDNA copy number without altering mitochondrial network length and morphology

A) Z-projections of SI microscopic images of paraformaldehyde-fixed diploid WT and Δ*mrx6* cells. Mitochondria were visualized by mitochondria-targeted dsRed protein (mt-dsRed). LacI-GFP marks mtDNA. Cells were grown in SD-ura-trp.

B, C, D, E) Number of end points (B), branch points (C), length of mitochondrial network (D) and mtDNA copy number normalized to mitochondrial network length (E) in WT and Δ*mrx6* cells. Analysis was performed on three-dimensional images (58 cells for WT, 69 cells for Δ*mrx6*).

F) Histogram showing distribution of distances between neighboring mtDNA copies in WT and Δ*mrx6* cells in three-dimensional images. Means of distance between mtDNA copies 692 nm and 872 nm for Δ*mrx6* and WT cells, respectively ($p<0.001$).

Figure 4

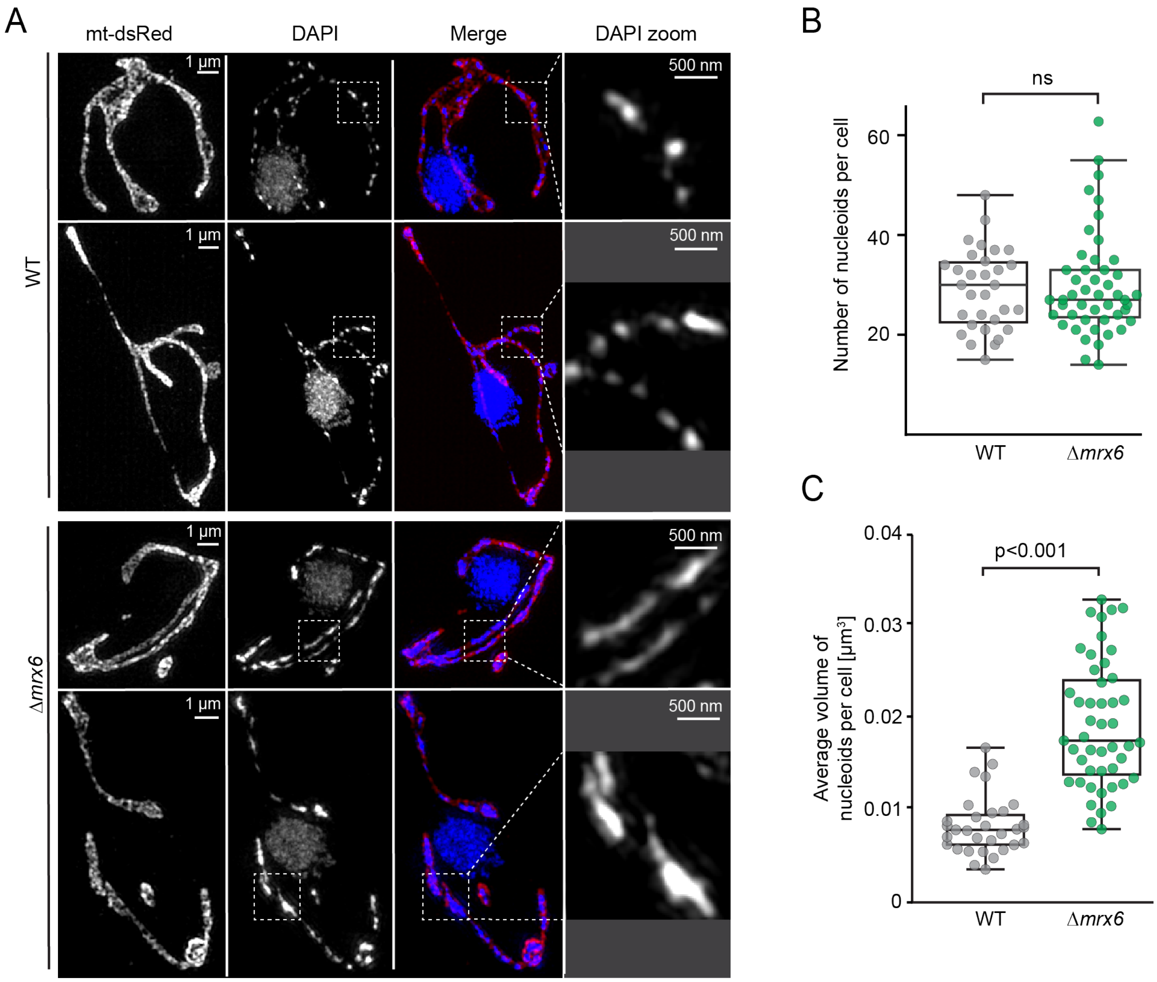

Figure 4: Δ*mrx*6 cells display elongated nucleoids

A) Z-projections of SI microscopic images of paraformaldehyde and methanol-fixed diploid cells that were stained with DAPI. Mitochondria were visualized by mt-dsRED. Cells were grown in SD-ura-trp.
B) Number and C) average volume of nucleoids stained with DAPI in WT and Δ*mrx6* cells. Analysis was performed on three-dimensional images. (31 cells for WT, 47 cells for Δ*mrx6*)

Figure 5

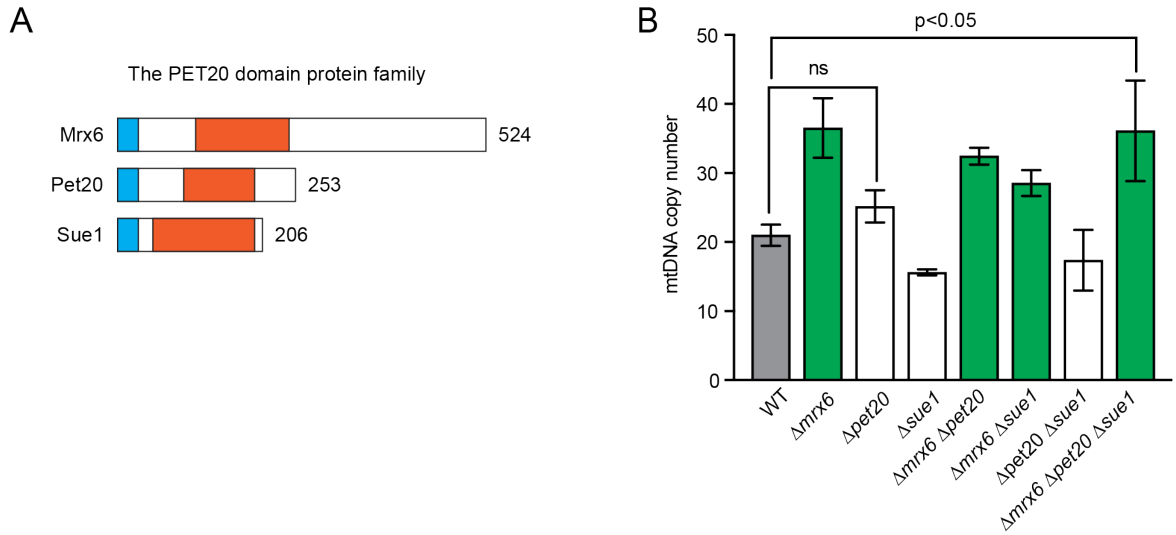

Figure 5: Mrx6 is a member of the PET20-domain containing protein family

A) Domain architecture of Mrx6 and other PET20-domain containing proteins. Blue indicates mitochondrial targeting sequences. Orange represents PET20-domain.
B) Analysis of mtDNA copy number of single, double and triple deletion mutants of *MRX6, PET20* and *SUE1,* measured by qPCR. Error bars are SD (n=2). Cells were grown in YPD.

Figure 6

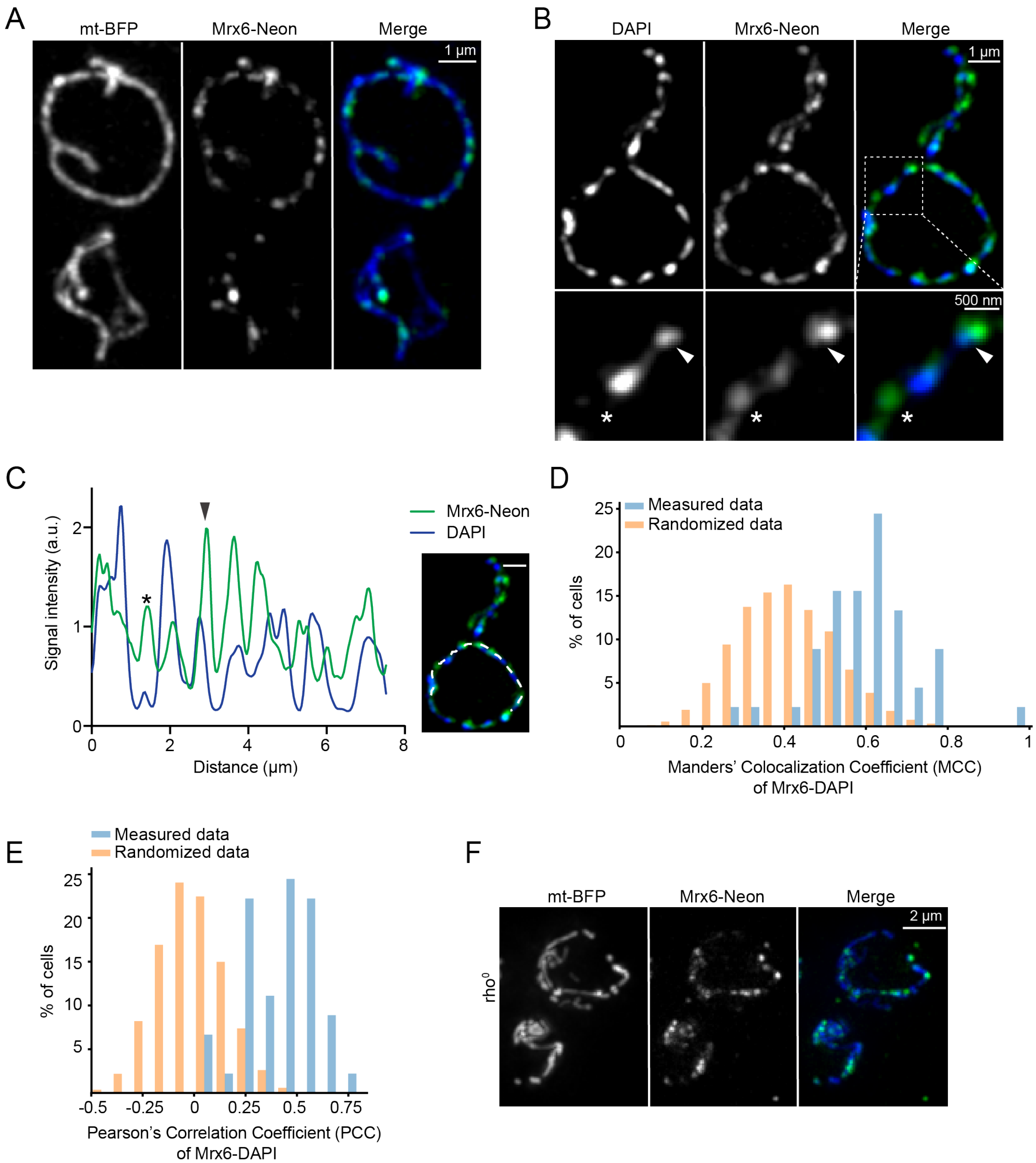

Figure 6: Mrx6 forms foci in mitochondria and colocalizes with mtDNA

A) Z-projection of microscopic images of a live cell expressing Mrx6-Neon. Mitochondria were visualized by mt-BFP. Mrx6-Neon (green), mt-BFP (blue) in the merged image. Cells were grown in SD-ura-trp.

B) Z-projections of microscopic images of a live cell expressing Mrx6-Neon (green). mtDNA was stained with DAPI (blue). Arrowhead shows colocalization of Mrx6-Neon and DAPI; asterisk marks non-colocalization. Cells were grown in SD-trp.
C) Line scan analysis of mitochondrial network for the cell shown in Fig. 6B.
D) Distribution of Manders' Colocalization Coefficients (MCC) calculated for colocalization of Mrx6-Neon with DAPI in 47 cells (mean=0.60) or in same line scans where the DAPI signal was randomized (mean=0.42, $p<0.001$).
E) Distribution of Pearson's Correlation Coefficients (PCC) determined for Mrx6-Neon and DAPI line scans in measured data (n=47 cells, mean=0.40) and in randomized data (mean=0, p= $p<0.001$).
F) Z-projection of microscopic images of a live cell that lacks mtDNA but expresses Mrx6-Neon (green). Mitochondria were visualized by mt-BFP (blue). Cells were grown in SD-ura.

Figure 7

A

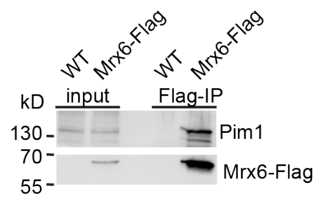

B

Mrx6-Flag immunoprecipitation

Total spectral count

	WT	Mrx6-Flag	*Δpet20* Mrx6-Flag	*Δsue1* Mrx6-Flag
Pim1	0	555	354	434
Mrx6	0	151	98	114
Pet20	0	44	0	44
Mam33	0	66	44	42

C

Pet20-Flag immunoprecipitation

Total spectral count

	WT	Pet20-Flag	*Δmrx6* Pet20-Flag	*Δsue1* Pet20-Flag
Pim1	0	391	6	484
Mrx6	0	67	0	86
Pet20	0	50	21	67
Mam33	0	39	0	46

D

Sue1-Flag immunoprecipitation

Total spectral count

	WT	Sue1-Flag	*Δpet20* Sue1-Flag	*Δmrx6* Sue1-Flag
Pim1	0	59	55	41
Mrx6	0	0	0	0
Pet20	0	0	0	0
Mam33	0	0	0	0
Sue1	0	3	4	3

Figure 7: Mrx6 binds to Pet20, Pim1 and Mam33

A) Western Blot analyses of an anti-Flag immunoprecipitation experiment from cells expressing Mrx6-Flag or Mrx6 (WT). Membranes were probed with antibodies against Pim1 (top) and the Flag-epitope (bottom). Cells were grown in YPD.
B) Interaction partners of Mrx6-Flag in cells expressing Mrx6-Flag; expressing Mrx6-Flag but lacking Pet20 or Sue1, identified by anti-Flag immunoprecipitations and mass spectrometry analyses. The numbers represent total spectral count. Cells were grown in YPD.
C) Interaction partners of Pet20-Flag in cells expressing Pet20-Flag; expressing Pet20-Flag but lacking Mrx6 or Sue1. Same as above.
D) Interaction partners of Sue1-Flag in cells expressing Sue1-Flag; expressing Sue1-Flag but lacking Mrx6 or Pet20. Same as above.

Figure 8

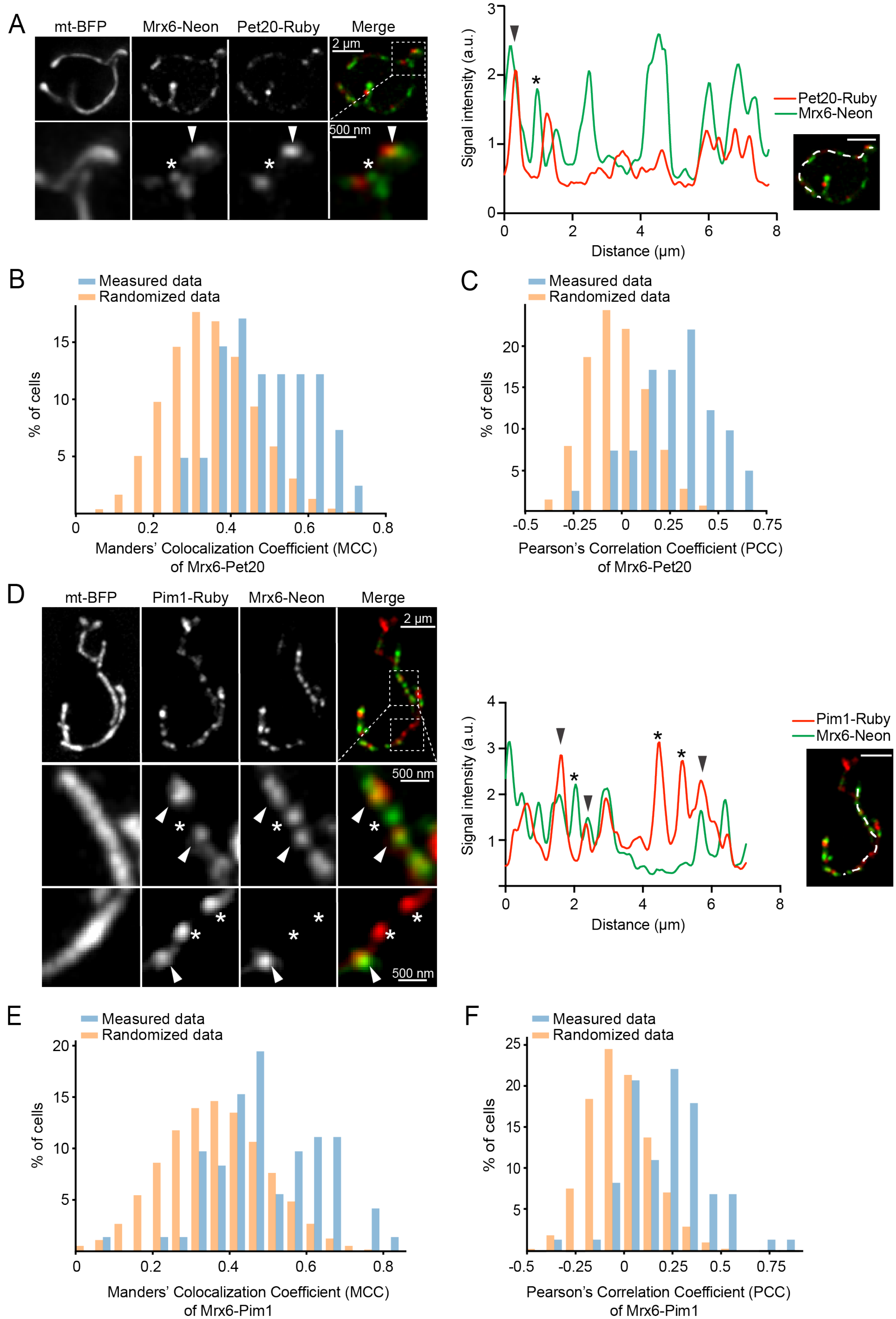

A
mt-BFP
Mrx6-Neon
Pet20-Ruby
Merge
2 µm
500 nm
Signal intensity (a.u.)
Distance (µm)
Pet20-Ruby
Mrx6-Neon
B
Measured data
Randomized data
% of cells
Manders' Colocalization Coefficient (MCC)
of Mrx6-Pet20
C
Measured data
Randomized data
% of cells
Pearson's Correlation Coefficient (PCC)
of Mrx6-Pet20
D
mt-BFP
Pim1-Ruby
Mrx6-Neon
Merge
2 µm
500 nm
500 nm
Signal intensity (a.u.)
Distance (µm)
Pim1-Ruby
Mrx6-Neon
E
Measured data
Randomized data
% of cells
Manders' Colocalization Coefficient (MCC)
of Mrx6-Pim1
F
Measured data
Randomized data
% of cells
Pearson's Correlation Coefficient (PCC)
of Mrx6-Pim1

Figure 8: Mrx6 partially colocalizes with Pet20 and Pim1

A) Z-projections of microscopic images of a live cell expressing Mrx6-Neon (green), and Pet20-Ruby (red). Line scan analysis of mitochondrial network is shown on the right. Arrowhead indicates colocalization of Mrx6-Neon and Pet20-Ruby; asterisk marks non-colocalization. Cells were grown in SD-ura-trp.
B) Distribution of Manders' Colocalization Coefficients (MCC) determined for colocalization of Mrx6-Neon with Pet20-Ruby in measured (n=41 cells, mean=0.50) and randomized data (mean=0.36, $p<0.001$).
C) Distribution of Pearson's Correlation Coefficients (PCC) between Mrx6-Neon and Pet20-Ruby in measured (n=41 cells, mean=0.28) and randomized data (mean=0, $p<0.001$).
D) Z-projections of microscopic images of a live cell expressing Mrx6-Neon (green), and Pim1-Ruby (red). Line scan analysis of mitochondrial network is shown on the right. Arrowhead indicates colocalization of Mrx6-Neon and Pim1-Ruby; asterisk marks non-colocalization. Cells were grown in SD-ura-trp.
E) Distribution of Manders' Colocalization Coefficients (MCC) determined for colocalization of Mrx6-Neon with Pim1-Ruby in measured (n=69 cells, mean=0.50) and randomized data (mean=0.37, $p<0.001$).
F) Distribution of Pearson's Correlation Coefficients (PCC) between Mrx6-Neon and Pim1-Ruby in measured (n=69 cells, mean=0.22) and randomized data (mean=0, $p<0.001$).

Figure 9

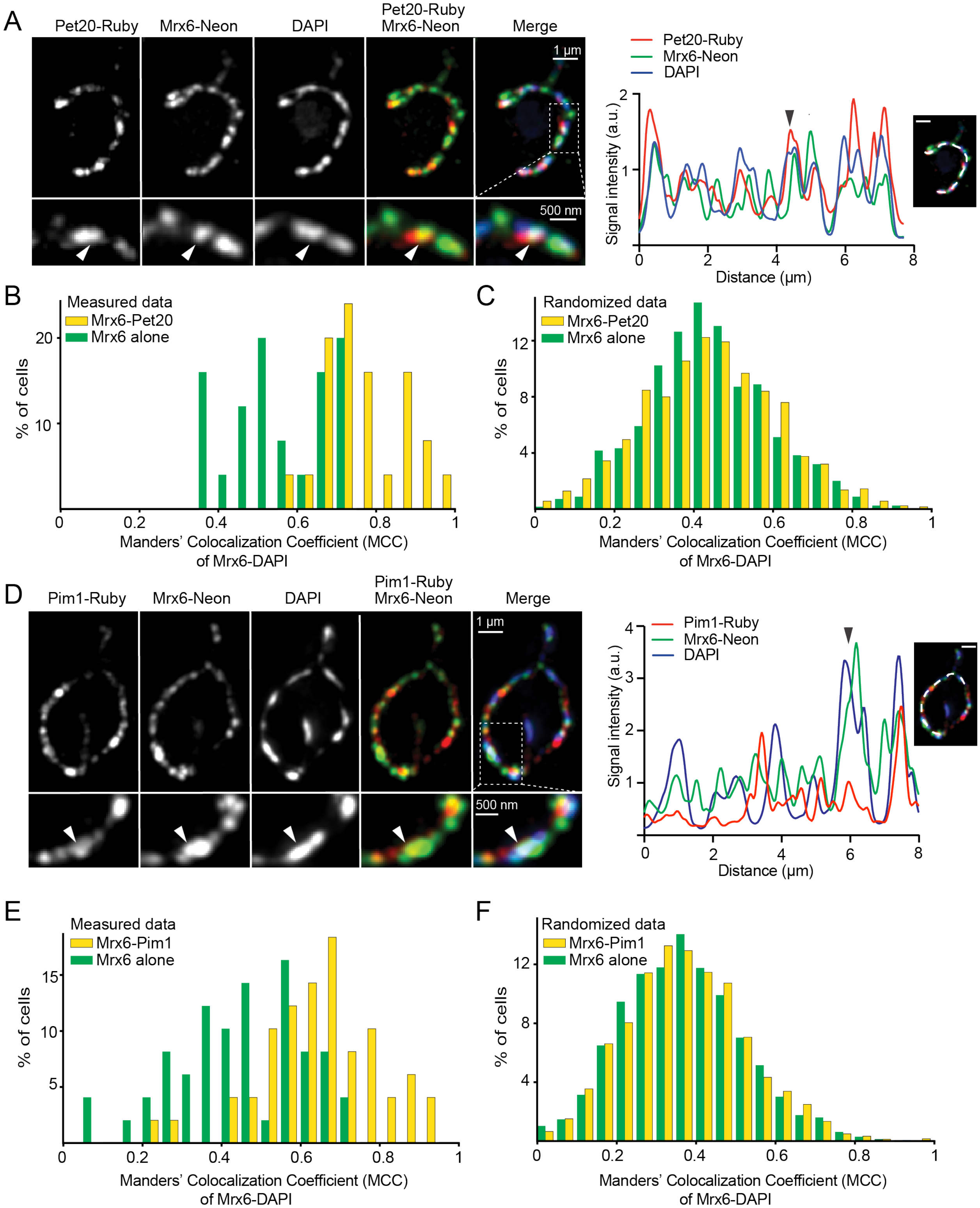

Figure 9: Mrx6 colocalizes with Pet20 and Pim1 in regions close to mtDNA

A) Z-projections of microscopic images of a live cell expressing Mrx6-Neon and Pet20-Ruby. mtDNA was stained with DAPI. Mrx6-Neon (green), Pet20-Ruby (red), and DAPI (blue) in the merged images. Line scan analysis of mitochondrial network is shown on the right. Arrowhead indicates colocalization of Mrx6-Neon, Pet20-Ruby and DAPI signal. Cells were grown in SD-trp.
B) Distribution of Manders' Colocalization Coefficients (MCC) determined for colocalization of Mrx6-Pet20 (Mrx6-Neon colocalizing with Pet20-Ruby) with DAPI signal (n=25 cells, mean=0.77); and Mrx6 alone (not colocalizing with Pet20-Ruby) with DAPI signal (mean=0.56, p<0.001).
C) Distribution of Manders' Colocalization Coefficients (MCC) determined for colocalization of Mrx6-Pet20 (Mrx6-Neon colocalizing with Pet20-Ruby) with randomized DAPI signal (n=25 cells, mean=0.44); and Mrx6-Neon alone (not colocalizing with Pet20-Ruby) with randomized DAPI signal (mean=0.45, p=0.78).
D) Z-projections of microscopic images of a live cell expressing Mrx6-Neon (green) and Pim1-Ruby (red). mtDNA was stained with DAPI (blue). Line scan analysis of mitochondrial network is shown on the right. Arrowhead indicates colocalization of Mrx6-Neon, Pim1-Ruby and DAPI signal. Cells were grown in SD-trp.
E) Distribution of Manders' Colocalization Coefficients (MCC) determined for colocalization of Mrx6-Pim1 (Mrx6-Neon colocalizing with Pim1-Ruby) with DAPI signal (n=49 cells, mean=0.65) and Mrx6 alone (not colocalizing with Pim1-Ruby) with DAPI signal (mean=0.46, p<0.001).
F) Distribution of Manders' Colocalization Coefficient (MCC) determined for colocalization of Mrx6-Pim1 (Mrx6-Neon colocalizing with Pim1-Ruby) with randomized DAPI signal (n=49 cells, mean=0.38); and Mrx6 alone (not colocalizing with Pim1-Ruby) with randomized DAPI signal (mean=0.37, p=0.49).

Figure 10

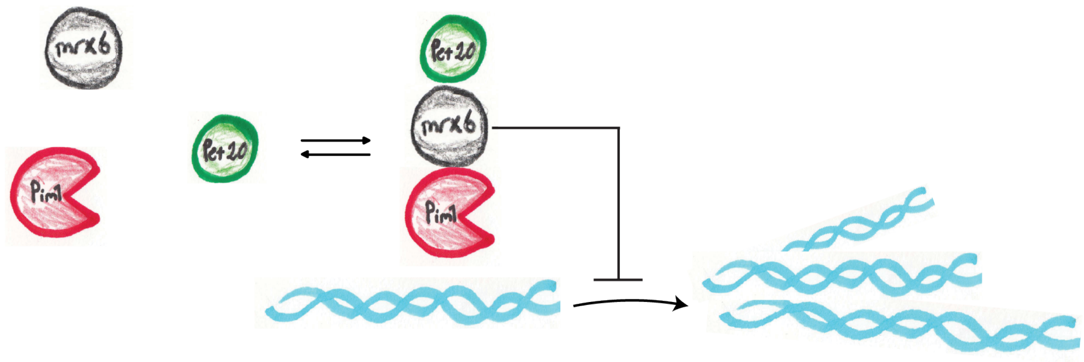

Figure 10: The Mrx6 complex colocalizes with mtDNA

Mrx6, Pet20 and Pim1 are present in distinct sub-complexes within mitochondria. The Mrx6 Complex (Mrx6, Pet20, Pim1) colocalizes preferentially with mtDNA, whereas single components are more often found in areas that lack mtDNA. The Mrx6 Complex might determine mtDNA levels through regulation of Pim1-mediated proteolysis.

Supp. Figure 1

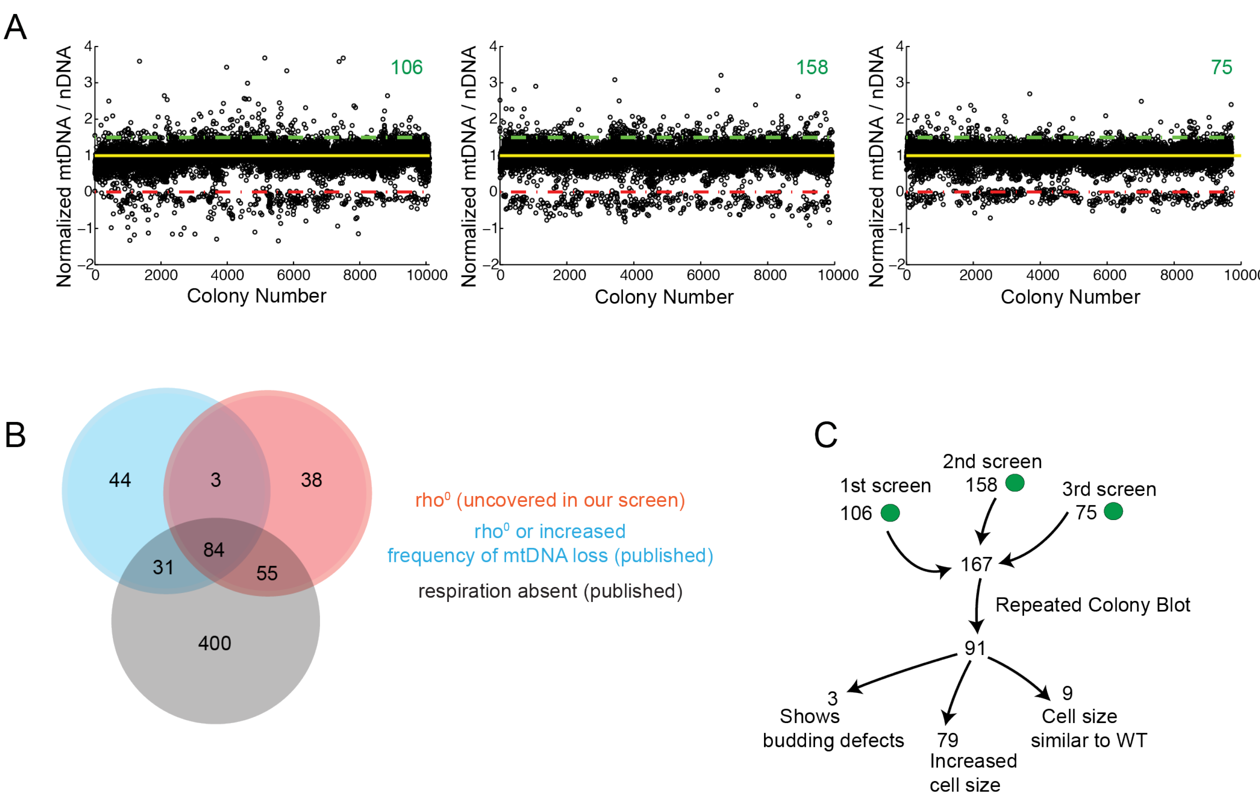

Supplementary Figure 1: Overview of colony blot screens

A) Scatter plots from three colony blot screens showing normalized mtDNA levels. In each screen, 5148 mutants of the deletion library were screened as replicates, resulting in 10296 colonies. Mutants above the green dashed line have at least 50% increase in mtDNA levels. The numbers of mutants (elevated mtDNA phenotype) identified in each screen are indicated on each plot (See Supp. Table 1.1 for the list of the mutants). Mutants below red dashed line, 180, lost majority of their mtDNA or lack completely. See Supp. Table 1.2 for their list.
B) Comparison of rho^0 mutants (shown as red) discovered in our screen with published literature. A list of mutants previously implicated in the maintenance of mtDNA (shown as blue) or respiratory growth (shown as black), were obtained from the Yeast Genome Database: (http://www.yeastgenome.org/phenotype/absent_mitochondrial_genome_maintenance/overview, http://www.yeastgenome.org/phenotype/abnormal_mitochondrial_genome_maintenance/overview, http://www.yeastgenome.org/reference/S000131621/overview, http://www.yeastgenome.org/phenotype/absent_respiratory_growth/overview)
C) Flow chart of the screen, showing number of mutants identified in each step. Initial hits from 3 independent screens were pooled (167) and subjected to a secondary colony blot experiment. The 91 candidates were selected and then subjected to qPCR and flow cytometry experiments (Supp. Table 1.4).

Supp. Figure 2

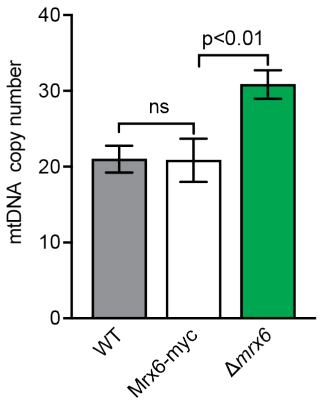

Supplementary Figure 2: Mrx6-myc retains its function

Analysis of mtDNA levels in cells that express Mrx6-myc, determined by qPCR. Error bars indicate SD (n=4).

Supp. Figure 3

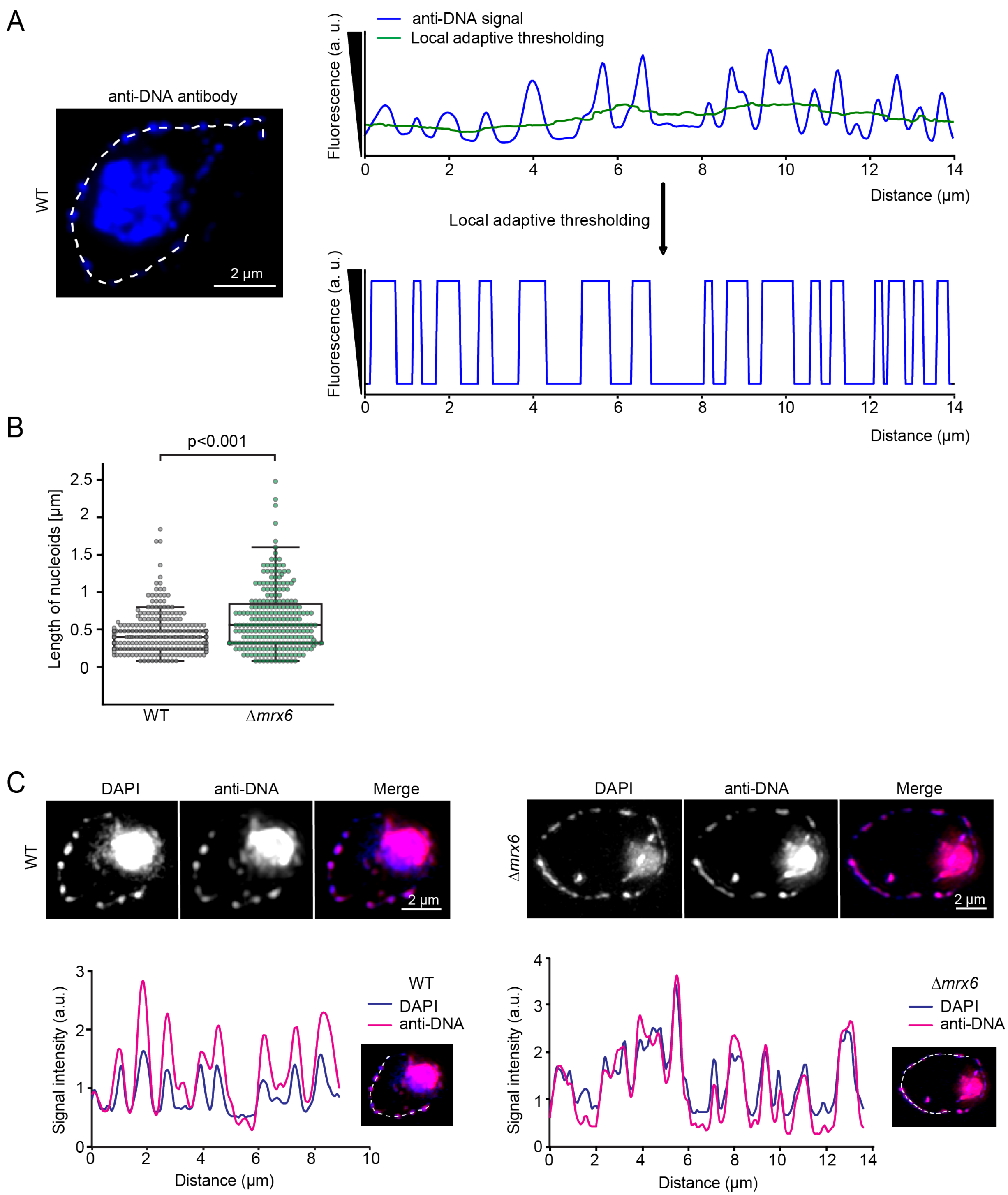

Supplementary Figure 3: Δ*mrx6* cells display elongated nucleoids

A) Z-projection of microscopic images of a fixed diploid WT cell, immunofluorescence by anti-DNA antibody (blue). Line scan analysis of the mitochondrial network is shown on the right. Length of nucleoids was determined from the intensity profile by adaptive thresholding.
B) Length of nucleoids in WT and Δ*mrx6* cells. (n=313 nucleoids for WT, 243 nucleoids for Δ*mrx6,* $p<0.001$, Welch's *t*-test).
C) Z-projections of microscopic images of fixed diploid WT and Δ*mrx6* cells, and their mitochondrial line scan comparisons of anti-DNA immunofluorescence and DAPI staining. Immunofluorescence by anti-DNA antibody (magenta) and DAPI (blue) shown in merge.

Supp. Figure 4

```
MRX6       MEHQALRRLVLYCPNFIRRGALRQNMTRVSCRHMSGKGGGRDEKGDCNEEKDSSKDLGR- 59
PET20      ----MLKLARPFIPPLSRNNAISSGIVLTSRRFQSSFTFLSN-----------QSLLSKN 45
SUE1       -------------------------MIL----------------------------LKRT 7

MRX6       -VPSKMKRAYDGETVIKEGDSHAESLAQQGKQPTDLAYNSRSKISGSNL------HLLVP 112
PET20      QMKSKRKKGSKKAAYHRQPPE-HEHTAPLIKQNKTITKKEHSDVRGSHLKKKRSDFSWLP 104
SUE1       -----KIRGVSVSFVSLQRRTHSRLVNPIRQQHQQITKQRSSKIL---KNAHFYDFRSLP 59

MRX6       RVASTDYISNKEVHTEGLFAGYRPLFLGNSGFPSDARKGKNFHELDDVLPNIQVVD--AS 170
PET20      RVPSTSHLKQSDMTTNVLYSGYRPLFINPNDPKLKEDTGS-------------------- 144
SUE1       KVPTTQYLEARELTRDILYSGYRPVMYPVKENPLFRDKKRKS--LQTLLTMNEKTNAEAK 117

MRX6       EKDGKLNVQEIIEDLQRT-SLRESIHSM--EQLPSSHKRKPVIPWDASISGMVYNDMPFK 227
PET20      --------------------------TLYEFAMKLEDLNEPLSPWISSATGLEFFS-EWE 177
SUE1       TIDEKKHKNILFGERGTGGIMSGGVNGTWKYNPTVPNELLPFNWWSTSSMGMEYFP-EWK 176

MRX6       YVPKNIILKMKPFKLLRIERKSQAK---NA-RKPTMIKL-----------QFHNRRI-ND 271
PET20      NIPSELLKNLKPFHPPKEKSMNTNELIHVSAKRNTLVDNKTSETLQRKMDEFSKRRGKGR 237
SUE1       NVPPYMMRKLKPFDKALQMRLTHKSKKKMK*----------------------------- 206

MRX6       TPELVNLYHNKSRLHESLYNTKPLQESGYSSANTSKRQKMLKARSDFEHKQKNYAYKHTF 331
PET20      KKSVVTLLQMKKKLEG*------------------------------------------- 253
SUE1       ------------------------------------------------------------ 206

MRX6       IKNDQELFRNELTKLNKILAREFKKLTKLSIHNEFKREHLPLAVYVSKSKGTKKLFRRSL 391
PET20      ------------------------------------------------------------ 253
SUE1       ------------------------------------------------------------ 206

MRX6       KMKIMDHIYPVYTTILSTLTNSRDSKKFENKIKAYIEKIIVRLSDEVPSTYFFQDGVDCI 451
PET20      ------------------------------------------------------------ 253
SUE1       ------------------------------------------------------------ 206

MRX6       IQPSPIHNFKRMHWLRYTKRHNTFWGRTIHKDVQVSFNDKYVVTRSGVRYTRYPTNLNTQ 511
PET20      ------------------------------------------------------------ 253
SUE1       ------------------------------------------------------------ 206

MRX6       LLETAFEEWDYYE*       524
PET20      --------------       253
SUE1       --------------       206
```

Supplementary Figure 4: Multiple sequence alignment of Mrx6, Pet20 and Sue1

Multiple sequence alignment of PET20-domain containing proteins by using Clustal Omega. Orange highlight marks PET20-domain.

Supp. Figure 5

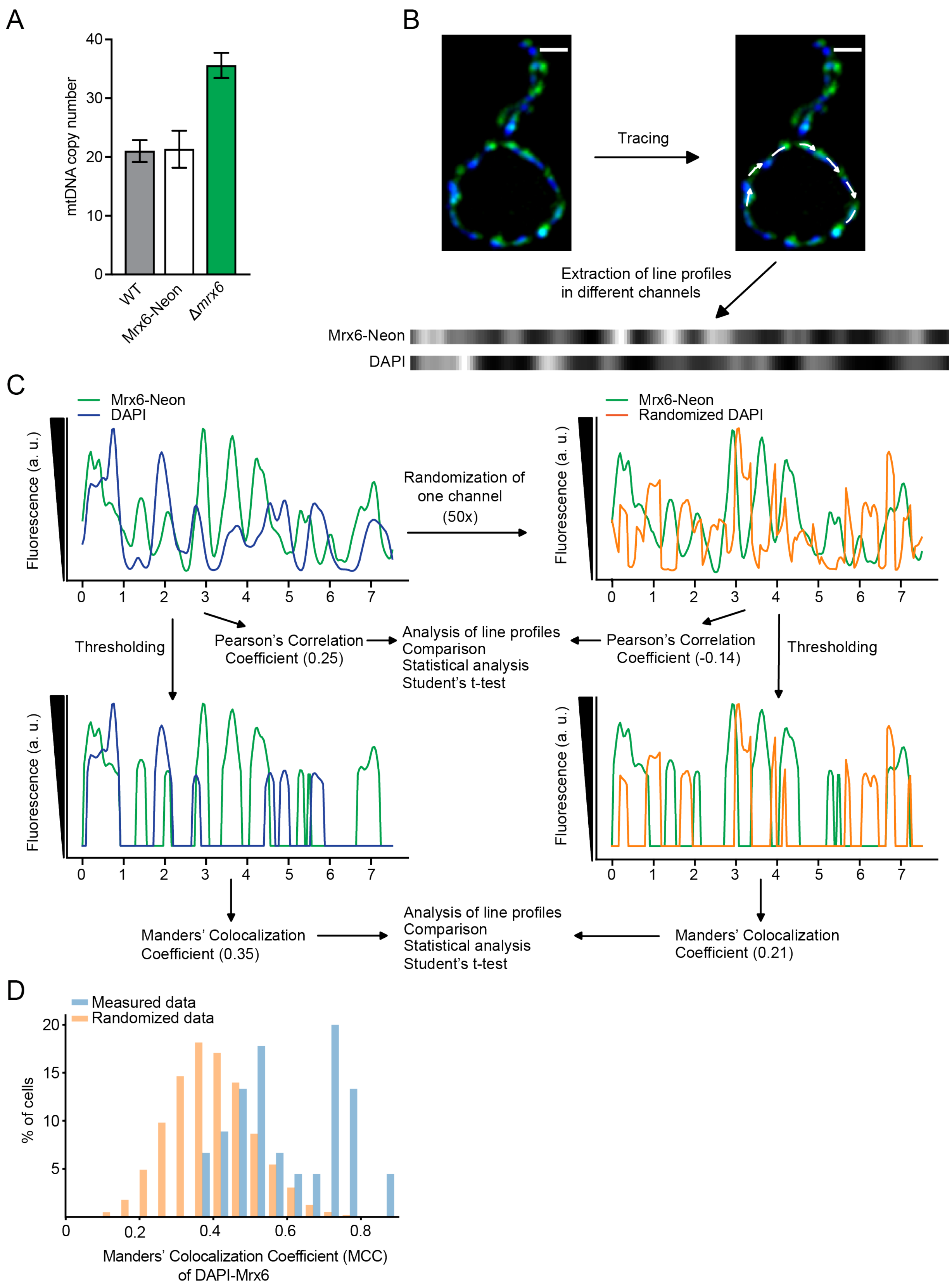

Supplementary Figure 5: Colocalization analysis of Mrx6 and mtDNA

A) Analysis of mtDNA levels in cells that express Mrx6-Neon, determined by qPCR. Error bars indicate SD (n=2), SD of Mrx6-Neon (n=3).
B) Z-projections of microscopic images of a live cell shown in Fig. 6B and showing the tracing of mitochondrial network and extraction of line profiles in different channels.
C) Colocalization analysis between line profiles of Mrx6-Neon (green) and DAPI (blue) for the cell shown in Supp. Fig. 5B by calculating Pearson's Correlation (PCC) and Manders' Colocalization Coefficients (MCC). Significance of these coefficients was tested by comparing them to PCC and MCC values calculated based on a randomized line profile (orange).
D) Distribution of Manders' Colocalization Coefficients (MCC) determined for colocalization of DAPI signal with Mrx6-Neon in measured (n=47 cells, mean=0.60); and in randomized data (mean=0.41, $p<0.001$).

Supp. Figure 6

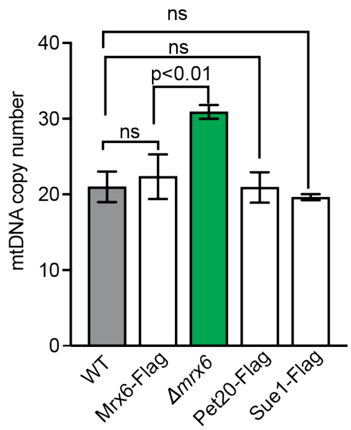

Supplementary Figure 6: Mrx6-Flag retains its function

Analysis of mtDNA levels in cells that express Mrx6-Flag, Pet20-Flag or Sue1-Flag, determined by qPCR. Error bars indicate SD (n=4), SD of Sue1-Flag (n=2).

Supp. Figure 7

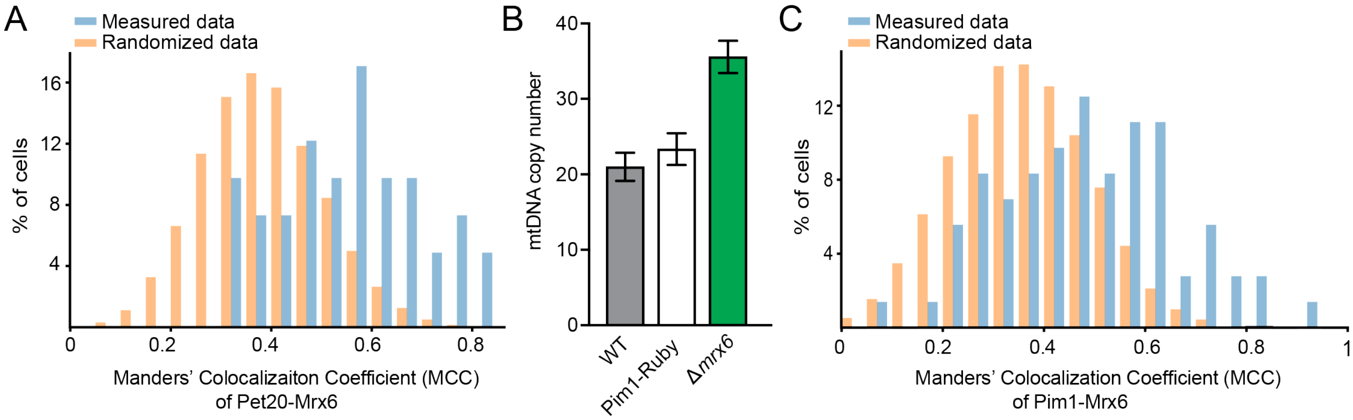

Supplementary Figure 7: Mrx6 partially colocalizes with Pet20 and Pim1

A) Distribution of Manders' Colocalization Coefficients (MCC) determined for colocalization of Pet20-Ruby with Mrx6-Neon in measured (n=41 cells, mean=0.56); and in randomized data (mean=0.39, p<0.001).
B) Analysis of mtDNA levels in cells that express Pim1-Ruby, determined by qPCR. Error bars indicate SD (n=2).
C) Distribution of Manders' Colocalization Coefficients (MCC) calculated for colocalization of Pim1-Ruby with Mrx6-Neon in measured (n=69 cells, mean=0.49); and in randomized data (mean=0.36, p<0.001).

Supp. Figure 8

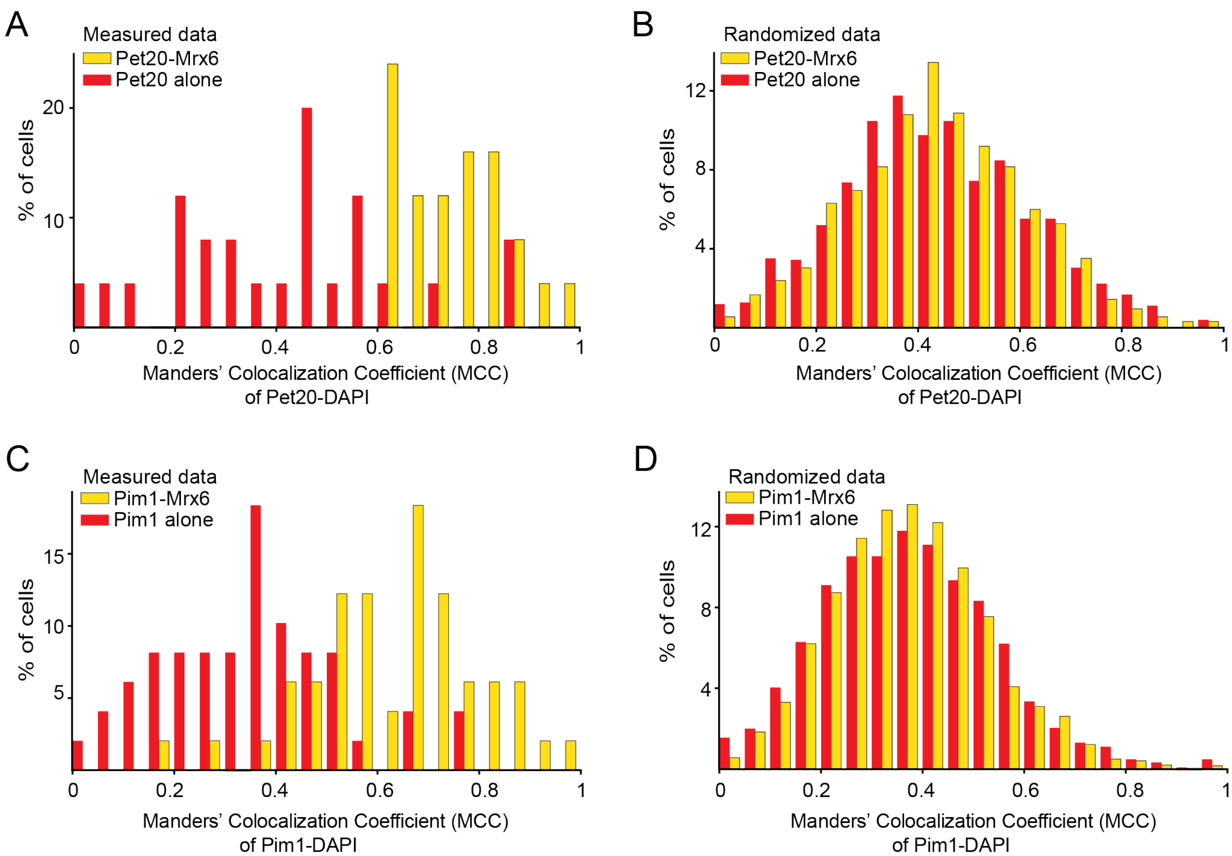

Supplementary Figure 8: Mrx6 colocalizes with Pet20 and Pim1 in regions close to mtDNA

A) Distribution of Manders' Colocalization Coefficients (MCC) determined for colocalization of Pet20-Mrx6 (Pet20-Ruby colocalizing with Mrx6-Neon) with DAPI signal (n=25 cells, mean=0.76); and Pet20 alone (not colocalizing with Mrx6-Neon) with DAPI signal (mean=0.42, p<0.001).
B) Distribution of Manders' Colocalization Coefficients (MCC) calculated for colocalization of Pet20-Mrx6 (Pet20-Ruby colocalizing with Mrx6-Neon) with randomized DAPI signal (n=25 cells, mean=0.44); and Pet20 alone (not colocalizing with Mrx6-Neon) with randomized DAPI signal (mean=0.44, p=0.79).
C) Distribution of Manders' Colocalization Coefficients (MCC) determined for colocalization of Pim1-Mrx6 (Pim1-Ruby colocalizing with Mrx6-Neon) with DAPI signal (n=49 cells, mean=0.64); and Pim1 alone (not colocalizing with Mrx6-Neon) with DAPI signal (mean=0.36, p<0.001).
D) Distribution of Manders' Colocalization Coefficients (MCC) calculated for colocalization of Pim1-Mrx6 (Pim1-Ruby colocalizing with Mrx6-Neon) with randomized DAPI signal (n=49 cells, mean=0.38); and Pim1 alone (not colocalizing with Mrx6-Neon) with randomized DAPI signal (mean=0.38, p=0.29).

Supp. Figure 9

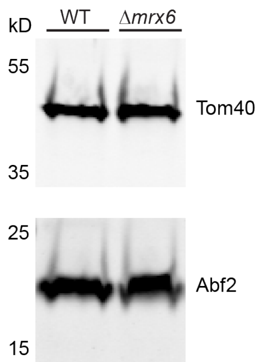

Supplementary Figure 9: Abf2 levels do not change after *MRX6* deletion

Western Blot showing Abf2 levels (bottom) in WT and Δ*mrx6* cells. Tom40 was used as a loading control (top).

Supp. Table 1.1 Mutants identified in each screen (increased mtDNA)

Screen 1	106 mutants	
YAL016W	YHR026W	YMR224C
YBL058W	YHR031C	YMR280C
YBR077C	YHR035W	YMR284W
YBR106W	YHR039C-B	YNL238W
YBR194W	YHR064C	YNL250W
YCL061C	YHR135C	YNL271C
YCR009C	YHR167W	YNL295W
YCR044C	YHR187W	YNR072W
YDL047W	YHR191C	YOL072W
YDL049C	YHR200W	YOL076W
YDL116W	YIL052C	YOR014W
YDR159W	YIL128W	YOR026W
YDR274C	YJL016W	YOR066W
YDR290W	YJL047C	YOR069W
YDR364C	YJL051W	YOR080W
YDR369C	YJL115W	YOR114W
YDR432W	YJL127C	YOR290C
YDR433W	YJR018W	YOR293W
YDR448W	YJR043C	YPL045W
YDR524C-B	YJR055W	YPL055C
YDR524W-A	YKL053W	YPL254W
YDR525W	YKL113C	YPR036W
YEL027W	YKR001C	YPR039W
YEL045C	YLL002W	YPR040W
YEL046C	YLL020C	YPR045C
YEL051W	YLR056W	YPR135W
YFL033C	YLR079W	
YGL020C	YLR176C	
YGL058W	YLR320W	
YGL084C	YLR399C	
YGL108C	YML001W	
YGL211W	YML028W	
YGL223C	YML032C	
YGL246C	YML058W	
YGR130C	YMR032W	
YGR159C	YMR038C	
YGR200C	YMR060C	
YGR252W	YMR100W	
YHL011C	YMR123W	
YHR021C	YMR190C	

Screen 2	158 mutants		
YAL047C	YDR363W	YHR154W	YML058W
YAL058W	YDR363W-A	YHR167W	YML080W
YBL039C	YDR364C	YIL008W	YMR038C
YBL071C-B	YDR369C	YIL024C	YMR179W
YBL071W-A	YDR414C	YIL076W	YMR224C
YBR106W	YDR432W	YIL087C	YMR284W
YBR173C	YDR433W	YIL128W	YMR307W
YBR174C	YDR448W	YJL047C	YMR312W
YBR194W	YDR485C	YJL115W	YNL021W
YBR196C-A	YDR532C	YJL127C	YNL072W
YBR284W	YEL027W	YJL139C	YNL119W
YBR289W	YEL051W	YJL176C	YNL133C
YCL016C	YER011W	YJR018W	YNL148C
YCL060C	YER074W	YJR104C	YNL199C
YCL061C	YER083C	YKL007W	YNL250W
YCR009C	YGL019W	YKL037W	YNL295W
YCR087C-A	YGL023C	YKL053W	YOL061W
YCR094W	YGL066W	YKL055C	YOL064C
YDL013W	YGL081W	YKL073W	YOL072W
YDL047W	YGL084C	YKL139W	YOR014W
YDL049C	YGL105W	YKL191W	YOR039W
YDL061C	YGL127C	YKL212W	YOR080W
YDL116W	YGL144C	YKR004C-A	YOR114W
YDL117W	YGL163C	YKR020W	YOR156C
YDL151C	YGL175C	YKR055W	YOR290C
YDL239C	YGL188C-A	YLL002W	YOR293W
YDR024W	YGL223C	YLR024C	YOR306C
YDR025W	YGL235W	YLR047C	YPL024W
YDR027C	YGL246C	YLR056W	YPL045W
YDR049W	YGR036C	YLR068W	YPL101W
YDR083W	YGR104C	YLR079W	YPL102C
YDR097C	YGR168C	YLR176C	YPL129W
YDR099W	YGR229C	YLR233C	YPL161C
YDR112W	YGR240C	YLR267W	YPL193W
YDR159W	YGR252W	YLR320W	YPR045C
YDR195W	YGR285C	YLR353W	YPR098C
YDR255C	YHL011C	YLR371W	YPR135W
YDR274C	YHR039C-B	YLR423C	YPR164W
YDR279W	YHR111W	YML028W	
YDR290W	YHR129C	YML032C	

Screen 3	75 mutants
YAL016C-B	YJR043C
YAL016W	YJR074W
YAL047C	YJR104C
YBL104C	YKL118W
YBR106W	YKL119C
YBR121C	YLL002W
YBR194W	YLR024C
YBR262C	YLR176C
YBR277C	YLR220W
YBR278W	YLR233C
YCL016C	YLR242C
YCL061C	YLR318W
YCR094W	YLR423C
YDL049C	YML032C
YDL081C	YML058W
YDR004W	YML080W
YDR097C	YMR038C
YDR195W	YMR100W
YDR363W-A	YMR179W
YDR369C	YMR224C
YDR414C	YMR284W
YEL027W	YNL148C
YEL045C	YNL273W
YEL051W	YOL145C
YEL061C	YOR080W
YGL108C	YOR114W
YGL127C	YOR359W
YGL163C	YPL045W
YGL186C	YPL101W
YGR020C	YPL102C
YHR026W	YPR044C
YHR031C	YPR045C
YHR039C-B	YPR120C
YHR134W	YPR135W
YHR191C	YPR164W
YIL128W	
YJL047C	
YJL115W	
YJL176C	
YJR015W	

Supp. Table 1.2 Mutants lacking mtDNA

180 mutants				
YAL048C	YDR298C	YHL004W	YML088W	YOR330C
YBL002W	YDR300C	YHR011W	YMR064W	YPL005W
YBL022C	YDR322W	YHR091C	YMR066W	YPL013C
YBL038W	YDR347W	YHR120W	YMR071C	YPL029W
YBL044W	YDR350C	YHR147C	YMR072W	YPL031C
YBL090W	YDR377W	YHR168W	YMR084W	YPL059W
YBR122C	YDR405W	YHR175W-A	YMR089C	YPL078C
YBR132C	YDR470C	YJL023C	YMR097C	YPL097W
YBR163W	YDR507C	YJL027C	YMR098C	YPL118W
YBR179C	YDR518W	YJL063C	YMR158W	YPL173W
YBR251W	YDR521W	YJL096W	YMR184W	YPL183W-A
YBR268W	YDR523C	YJL102W	YMR228W	YPL271W
YBR282W	YEL036C	YJL140W	YMR267W	YPR047W
YCR003W	YEL050C	YJR101W	YMR286W	YPR067W
YCR004C	YER014W	YJR113C	YMR287C	YPR100W
YCR024C	YER017C	YJR114W	YMR293C	YPR116W
YCR028C-A	YER050C	YJR122W	YNL005C	YBL012C
YCR046C	YER087W	YJR144W	YNL073W	YLR260W
YCR071C	YER103W	YKL003C	YNL081C	YPR099C
YDL040C	YER110C	YKL016C	YNL160W	YDL057W
YDL044C	YER122C	YKL134C	YNL170W	
YDL045W-A	YER154W	YKL155C	YNL177C	
YDL062W	YER169W	YKL169C	YNL184C	
YDL063C	YFL016C	YKL170W	YNL213C	
YDL146W	YFL036W	YKL194C	YNL252C	
YDL167C	YGL064C	YKR006C	YNL284C	
YDL181W	YGL095C	YLL006W	YNR036C	
YDL198C	YGL107C	YLL027W	YNR037C	
YDL202W	YGL129C	YLR069C	YOL033W	
YDR042C	YGL143C	YLR091W	YOL100W	
YDR065W	YGL220W	YLR114C	YOR150W	
YDR078C	YGL240W	YLR139C	YOR158W	
YDR079W	YGR101W	YLR148W	YOR187W	
YDR114C	YGR150C	YLR204W	YOR199W	
YDR175C	YGR165W	YLR270W	YOR200W	
YDR194C	YGR180C	YLR288C	YOR201C	
YDR237W	YGR215W	YLR312W-A	YOR205C	
YDR268W	YGR219W	YLR369W	YOR211C	
YDR295C	YGR220C	YLR382C	YOR241W	
YDR296W	YGR257C	YLR396C	YOR305W	

Supp. Table 1.3 Mutants pooled from 3 screens to be re-tested (increased mtDNA)

Gene name	167 mutants		
YAL058W	*YMR190C*	*YOR293W*	*YDR363W*
YEL061C	*YCR009C*	*YGR104C*	*YPR120C*
YLL002W	*YMR224C*	*YOR359W*	*YDR364C*
YER011W	*YLR176C*	*YOR114W*	*YPR135W*
YLR024C	*YMR284W*	*YOL064C*	*YDR369C*
YGR168C	*YLR220W*	*YOR156C*	*YPR164W*
YLR047C	*YMR307W*	*YOL072W*	*YDR414C*
YHR031C	*YKL007W*	*YJL176C*	*YCR094W*
YLR056W	*YNL295W*	*YOL076W*	*YDR004W*
YHR035W	*YKL037W*	*YLR233C*	*YGR252W*
YLR068W	*YNL273W*	*YPL254W*	*YDR025W*
YHR111W	*YKL053W*	*YLR318W*	*YAL016C-B*
YLR079W	*YNL271C*	*YJL115W*	*YBR278W*
YHR129C	*YKL055C*	*YFL033C*	*YBL071C-B*
YML080W	*YOR014W*	*YJL047C*	*YBR284W*
YHR134W	*YKL073W*	*YDR433W*	*YBL071W-A*
YML058W	*YIL052C*	*YHL011C*	*YCR087C-A*
YHR154W	*YDR448W*	*YHR187W*	*YDR524W-A*
YML032C	*YHR039C-B*	*YHR026W*	*YJR018W*
YHR167W	*YDR525W*	*YMR032W*	*YGL188C-A*
YGL058W	*YHR191C*	*YLR423C*	*YJR043C*
YBL104C	*YDR532C*	*YGL223C*	*YCL061C*
YGL084C	*YMR312W*	*YMR060C*	*YDL116W*
YBR077C	*YGL105W*	*YLR399C*	*YGL186C*
YNL148C	*YNL250W*	*YAL047C*	*YDL117W*
YNL133C	*YGL108C*	*YPL045W*	*YJL016W*
YKR001C	*YMR100W*	*YGL235W*	*YDL151C*
YIL128W	*YGL127C*	*YPL024W*	*YOL145C*
YKR020W	*YPR036W*	*YJR074W*	*YDR432W*
YNL119W	*YGL163C*	*YAL016W*	*YDR363W-A*
YKR055W	*YPR044C*	*YJR104C*	*YEL027W*
YKL139W	*YDL047W*	*YHR021C*	*YBL039C*
YDR255C	*YPR045C*	*YPL161C*	*YEL045C*
YJR055W	*YMR038C*	*YLR320W*	*YGL019W*
YDR274C	*YJL127C*	*YPL129W*	*YEL051W*
YBR106W	*YBR173C*	*YDR159W*	
YDR290W	*YOR026W*	*YPL101W*	
YDL049C	*YKL113C*	*YDR195W*	
YIL024C	*YOR039W*	*YPL102C*	
YDL081C	*YKL118W*	*YGL246C*	
YML028W	*YOR080W*	*YBR194W*	
YCL016C	*YKL119C*	*YGR020C*	
YMR179W	*YOR290C*	*YDR097C*	
YCL060C	*YGR036C*	*YPL055C*	

Supp. Table 1.4 Mutants selected for mtDNA copy number (qPCR) and cell size analysis

relative mtDNA			relative cell size		relative mtDNA			relative cell size	
Gene name	qPCR	SEM (qPCR)	SSC-H	SEM (SSC-H)	Gene name	qPCR	SEM (qPCR)	SSC-H	SEM (SSC-H)
YLL002W	2.31	0.11	1.74	0.002	*YOL064C*	1.99	0.09	1.24	0.017
YLR024C	1.26	0.03	1.12	0.082	*YOL072W*	1.86	0.00	1.34	0.035
YLR079W	1.90	0.17	2.01	0.069	*YJL176C*	2.83	0.22	2.99	0.097
YML058W	1.30	0.10	1.15	0.048	*YOL076W*	2.26	0.22	1.12	0.070
YML032C	2.17	0.07	1.56	0.012	*YLR233C*	2.08	0.33	1.69	0.036
YGL058W	2.18	0.05	1.20	0.002	*YPL254W*	2.41	0.26	3.07	0.167
YBR077C	1.55	0.09	1.21	0.054	*YLR318W*	2.58	0.15	1.32	0.027
YNL148C	2.20	0.25	1.74	0.166	*YJL115W*	3.43	0.01	1.77	0.037
YKR001C	1.54	0.02	1.21	0.088	*YJL047C*	2.45	0.03	1.30	0.049
YIL128W	2.07	0.22	1.14	0.057	*YDR433W*	2.84	0.17	1.78	0.077
YKR055W	1.56	0.01	2.36	0.035	*YMR032W*	2.00	0.09	1.41	0.034
YKL139W	1.84	0.07	1.44	0.090	*YGL223C*	1.91	0.09	1.25	0.057
YJR055W	1.39	0.05	1.08	0.087	*YMR060C*	1.25	0.10	1.07	0.006
YDR290W	1.36	0.03	1.19	0.024	*YLR399C*	1.20	0.11	1.58	0.001
YDL049C	1.68	0.09	1.08	0.008	*YAL047C*	2.42	0.17	2.64	0.014
YML028W	1.67	0.16	1.15	0.027	*YPL045W*	2.91	0.15	1.60	0.219
YCL016C	1.80	0.05	1.48	0.039	*YPL024W*	1.67	0.14	1.23	0.046
YMR190C	1.41	0.15	1.12	0.017	*YJR074W*	2.21	0.27	2.12	0.013
YBR106W	1.95	0.12	1.76	0.019	*YAL016W*	3.09	0.30	1.70	0.282
YLR176C	1.74	0.06	1.09	0.005	*YJR104C*	2.02	0.14	1.40	0.005
YMR284W	1.33	0.04	1.10	0.024	*YLR320W*	3.44	0.08	2.43	0.133
YMR307W	2.19	0.05	3.67	0.180	*YPL129W*	1.38	0.05	2.20	0.067
YNL295W	2.42	0.13	1.05	0.003	*YDR159W*	2.01	0.16	1.67	0.007
YNL273W	1.19	0.17	1.18	0.025	*YPL101W*	1.82	0.01	1.47	0.024
YKL053W	1.78	0.28	1.40	0.008	*YDR195W*	1.89	0.28	2.33	0.023
YKL055C	1.79	0.24	1.22	0.032	*YGL246C*	1.73	0.09	1.13	0.094
YOR014W	1.52	0.03	1.37	0.045	*YDR097C*	1.72	0.08	1.19	0.043
YDR448W	1.82	0.07	1.01	0.039	*YPL055C*	1.84	0.09	1.14	0.021
YHR039C-B	2.53	0.56	1.26	0.125	*YDR364C*	2.41	0.37	1.87	0.202
YHR191C	1.92	0.12	1.52	0.032	*YPR135W*	3.07	0.02	2.03	0.009
YDR532C	2.32	0.07	1.58	0.120	*YDR369C*	2.78	0.54	1.60	0.033
YMR312W	2.04	0.43	1.48	0.029	*YPR164W*	1.65	0.06	1.32	0.051
YMR100W	1.49	0.27	1.07	0.005	*YGR252W*	1.50	0.08	0.98	0.067
YGL163C	2.00	0.19	1.27	0.034	*YBR284W*	1.19	0.02	1.12	0.015
YPR044C	1.62	0.06	1.64	0.187	*YBL071W-A*	1.66	0.16	1.69	0.107
YDL047W	2.15	0.06	1.60	0.149	*YJR018W*	1.50	0.16	1.20	0.073
YPR045C	1.76	0.15	1.61	0.072	*YJR043C*	1.93	0.04	1.26	0.013
YMR038C	2.18	0.28	1.13	0.057	*YCL061C*	1.92	0.20	1.44	0.001
YJL127C	3.18	0.14	2.03	0.018	*YDL116W*	2.45	0.47	1.66	0.063
YBR173C	1.23	0.19	1.57	0.109	*YDL117W*	1.37	0.10	1.90	0.028
YOR026W	2.67	0.10	1.48	0.009	*YOL145C*	2.05	0.29	1.40	0.004
YKL113C	2.69	0.51	1.25	0.002	*YEL051W*	1.80	0.07	1.14	0.122
YOR080W	4.27	0.29	2.06	0.040	*YBR194W*	1.39	0.09	1.02	0.012
YKL119C	1.97	0.04	1.25	0.134	*YDR004W*	1.45	0.31	1.30	0.068
YOR290C	1.51	0.19	1.55	0.075	*YEL027W*	2.13	0.02	1.22	0.140
YOR114W	2.21	0.39	1.03	0.012					

Mutants selected for mtDNA (qPCR) and cell size analysis (total 90 mutants)
n=2 independent experiments
Values are normalized to WT.

Supp. Table 2. Yeast strains used/created in this study

Name	Short Description			Genotype	Source
PWY1933	WT *(mt-LacO-LacI pvt100u-mt-dsRed)*	W303	*mat a/α*	*mt-LacO leu2-3,112/leu2-3,112 trp1-1/TRP1 can1-100/ can1-100 ura3-1/ura3-1 ade2-1/ADE2 his3-11,15/his3-11,15 HO-mt-3xGFP-LacI-kanMx-HO pvt100u-mt-dsRed*	1
PWY2114	*Δmrx6 (mt-LacO-LacI pvt100u-mt-dsRed)*	W303	*mat a/α*	*mt-LacO Δmrx6::HphNT1/Δmrx6::HphNT1# leu2-3,112/leu2-3,112 TRP1/TRP1 can1-100/ can1-100 ura3-1/ura3-1 ade2-1/ADE2 his3-11,15/his3-11,15 HO-mt-3xGFP-LacI-kanMx-HO pvt100u-mt-dsRed*	This study.
PWY2115	WT	W303	*mat a*	*mt-LacO leu2-3,112 can1-100 ura3-1 his3-11,15*	This study.
PWY2116	*Δmrx6*	W303	*mat a*	*mt-LacO Δmrx6::HphNT1# leu2-3,112 can1-100 ura3-1 his3-11,15*	This study.
PWY2117	*Mrx6-myc*	W303	*mat a*	*mt-LacO mrx6-c-myc:HphNT1 leu2-3,112 trp1-1 can1-100 ura3-1 his3-11,15*	This study.
PWY2118	*Δpet20*	W303	*mat a*	*mt-LacO Δpet20::HIS3+ leu2-3,112 can1-100 ura3-1 his3-11,15*	This study.
PWY2119	*Δsue1*	W303	*mat a*	*mt-LacO Δsue1::NatNT2* leu2-3,112 can1-100 ura3-1 his3-11,15*	This study.
PWY2120	*Δpet20 Δsue1*	W303	*mat a*	*mt-LacO Δpet20::HIS3+ Δsue1::NatNT2* leu2-3,112 can1-100 ura3-1 his3-11,15*	This study.
PWY2121	*Δmrx6 Δsue1*	W303	*mat a*	*mt-LacO Δmrx6::HphNT1# Δsue1::NatNT2* leu2-3,112 can1-100 ura3-1 his3-11,15*	This study.
PWY2122	*Δmrx6 Δpet20*	W303	*mat a*	*mt-LacO Δmrx6::HphNT1# Δpet20::HIS3+ leu2-3,112 can1-100 ura3-1 his3-11,15*	This study.
PWY2123	*Δmrx6 Δpet20 Δsue1*	W303	*mat a*	*mt-LacO Δmrx6::HphNT1# Δpet20::HIS3+ Δsue1::NatNT2* leu2-3,112 can1-100 ura3-1 his3-11,15*	This study.
PWY2124	*Pet20-Flag*	W303	*mat a*	*mt-LacO Pet20-3xFlag:kanMx leu2-3,112 can1-100 ura3-1 his3-11,15*	This study.

Name	Short Description			Genotype	Source
PWY2125	*Mrx6-Flag*	W303	*mat a*	*mt-LacO Mrx6-3xFlag:kanMx leu2-3,112 can1-100 ura3-1 his3-11,15*	This study.
PWY2126	*Sue1-Flag*	W303	*mat a*	*mt-LacO Sue1-3xFlag:kanMx leu2-3,112 can1-100 ura3-1 his3-11,15*	This study.
PWY2127	*Sue1-Flag Δmrx6*	W303	*mat a*	*mt-LacO Sue1-3xFlag:kanMx Δmrx6::HphNT1*$^{\#}$ *leu2-3,112 can1-100 ura3-1 his3-11,15*	This study.
PWY2128	*Sue1-Flag Δpet20*	W303	*mat a*	*mt-LacO Sue1-3xFlag:kanMx Δpet20::HIS3*$^{+}$ *leu2-3,112 can1-100 ura3-1 his3-11,15*	This study.
PWY2129	*Pet20-Flag Δsue1*	W303	*mat a*	*mt-LacO Pet20-3xFlag:kanMx Δsue1::NatNT2* leu2-3,112 can1-100 ura3-1 his3-11,15*	This study.
PWY2130	*Pet20-Flag Δmrx6*	W303	*mat a*	*mt-LacO Pet20-3xFlag:kanMx Δmrx6::HphNT1*$^{\#}$ *leu2-3,112 can1-100 ura3-1 his3-11,15*	This study.
PWY2131	*Mrx6-Flag Δpet20*	W303	*mat a*	*mt-LacO Mrx6-3xFlag:kanMx Δpet20::HIS3*$^{+}$ *leu2-3,112 can1-100 ura3-1 his3-11,15*	This study.
PWY2132	*Mrx6-Flag Δsue1*	W303	*mat a*	*mt-LacO Mrx6-3xFlag:kanMx Δsue1::NatNT2* leu2-3,112 can1-100 ura3-1 his3-11,15*	This study.
PWY2133	*Mrx6-Neon*	W303	*mat a*	*mt-LacO Mrx6-mNeonGreen:kanMx leu2-3,112 can1-100 ura3-1 his3-11,15*	This study.
PWY2134	*Mrx6-Neon mtBFP*	W303	*mat a*	*mt-LacO Mrx6-mNeonGreen:kanMx leu2-3,112 can1-100 ura3-1 his3-11,15 pvt100u-mtTagBFP*	This study.
PWY2135	*rho*^{0} *Mrx6-Neon mtBFP*	W303	*mat a*	*Mrx6-mNeonGreen:kanMx leu2-3,112 trp1-1 can1-100 ura3-1 ade2-1 his3-11,15 pvt100u-mtTagBFP*	This study.
PWY2136	*Mrx6-Neon Pet20-Ruby*	W303	*mat a*	*mt-LacO Mrx6-mNeonGreen:kanMx Pet20-mRuby3:HIS3 leu2-3,112 can1-100 ura3-1 his3-11,15*	This study.
PWY2137	*Mrx6-Neon Pet20-Ruby mtBFP*	W303	*mat a*	*mt-LacO Mrx6-mNeonGreen:kanMx Pet20-mRuby3:HIS3 leu2-3,112 can1-100 ura3-1 his3-11,15 pvt100u-mtTagBFP*	This study.
PWY2138	*Pim1-Ruby*	W303	*mat a*	*mt-LacO Pim1-mRuby3:HIS3 leu2-3,112 can1-100 ura3-1 his3-11,15*	This study.

Name	Short Description			Genotype	Source
PWY2139	*Mrx6-Neon Pim1-Ruby*	W303	*mat a*	*mt-LacO Mrx6-mNeonGreen:kanMx Pim1-mRuby3:HIS3 leu2-3,112 can1-100 ura3-1 his3-11,15*	This study.
PWY2140	*Mrx6-Neon Pim1-Ruby mtBFP*	W303	*mat a*	*mt-LacO Mrx6-mNeonGreen:kanMx Pim1-mRuby3:HIS3 leu2-3,112 can1-100 ura3-1 his3-11,15 pvt100u-mtTagBFP*	This study.
PWY2172	*Δpim1 c1*	W303	*mat a*	*mt-LacO Δpim1::HphNT1*[#] *leu2-3,112 can1-100 ura3-1 his3-11,15*	This study.
PWY2173	*Δpim1 c2*	W303	*mat a*	*mt-LacO Δpim1::HphNT1*[#] *leu2-3,112 can1-100 ura3-1 his3 11,15*	This study.
PWY2174	*Δpim1 c3*	W303	*mat a*	*mt-LacO Δpim1::HphNT1*[#] *leu2-3,112 can1-100 ura3-1 his3-11,15*	This study.
PWY2175	*Δmrx6 Δpim1 c5*	W303	*mat a*	*mt-LacO Δpim1::HIS3*[+] *Δmrx6::HphNT1*[#] *leu2-3,112 can1-100 ura3-1 his3-11,15*	This study.
PWY2176	*Δmrx6 Δpim1 c7*	W303	*mat a*	*mt-LacO Δpim1::HIS3*[+] *Δmrx6::HphNT1*[#] *leu2-3,112 can1-100 ura3-1 his3-11,15*	This study.
PWY2177	*Δmrx6 Δpim1 c8*	W303	*mat a*	*mt-LacO Δpim1::HIS3*[+] *Δmrx6::HphNT1*[#] *leu2-3,112 can1-100 ura3-1 his3-11,15*	This study.
BY4741	WT	s288c	*mat a*	*his3Δ1 leu2Δ0 met15Δ0 ura3Δ0*	2
	Saccharomyces Gene Deletion Collection	s288c	*mat a*		3

[#] Deletion cassette amplified from pFA6a-HphNT1, * from pFA6a-NatNT2, and + from pFa6a-His3Mx (Janke C. et al., 2004).

[1] Osman, C., T.R. Noriega, V. Okreglak, J.C. Fung, and P. Walter. 2015. Integrity of the yeast mitochondrial genome, but not its distribution and inheritance, relies on mitochondrial fission and fusion. *Proc Natl Acad Sci U S A*. 112:E947-956.

[2] Brachmann, C.B., A. Davies, G.J. Cost, E. Caputo, J. Li, P. Hieter, and J.D. Boeke. 1998. Designer deletion strains derived from Saccharomyces cerevisiae S288C: a useful set of strains and plasmids for PCR-mediated gene disruption and other applications. *Yeast*. 14:115-132.

[3] http://sequence-www.stanford.edu/group/yeast_deletion_project/deletions3.html

Supp. Table 3. Plasmids used/created in this study

Name	Short Description	Marker	Resistance	Source
pPW744	p416ADH	*URA3*	Amp	1
pPW1067	pYM20-9xMyc tag	*HphNT1*	Amp	2
pPW1882	pVT100u-mtDsRed	*URA3*	Amp	3
pPW3075	pVT100u-mtTagBFP	*URA3*	Amp	4
pPW3317	pKT127-mNeonGreen	*kanMx*	Amp	This study, 5
pPW3318	pFa6a-mRuby3	*HIS3*	Amp	This study, 6
pPW3319	p416ADH-Mrx6-myc	*URA3*	Amp	This study.
pPW3320	pFa6a-GlySerGly-3xFlag	*kanMx*	Amp	This study.
pPW3321	pUC19-COX1		Amp	This study.
pPW3322	pUC19-ACT1		Amp	This study.
pPW3418	p416ADH-Pim1	*URA3*	Amp	This study.

[1] Mumberg, D., R. Muller, and M. Funk. 1995. Yeast vectors for the controlled expression of heterologous proteins in different genetic backgrounds. *Gene*. 156:119-122.

[2] Janke, C., M.M. Magiera, N. Rathfelder, C. Taxis, S. Reber, H. Maekawa, A. Moreno-Borchart, G. Doenges, E. Schwob, E. Schiebel, and M. Knop. 2004. A versatile toolbox for PCR-based tagging of yeast genes: new fluorescent proteins, more markers and promoter substitution cassettes. *Yeast*. 21:947-962.

[3] Murley, A., L.L. Lackner, C. Osman, M. West, G.K. Voeltz, P. Walter, and J. Nunnari. 2013. ER-associated mitochondrial division links the distribution of mitochondria and mitochondrial DNA in yeast. *eLife*. 2:e00422. Doi: 10.7554/eLife.00422

[4] Kornmann, B., E. Currie, S.R. Collins, M. Schuldiner, J. Nunnari, J.S. Weissman, and P. Walter. 2009. An ER-mitochondria tethering complex revealed by a synthetic biology screen. *Science*. 325:477-481.

[5] Shaner, N.C., G.G. Lambert, A. Chammas, Y. Ni, P.J. Cranfill, M.A. Baird, B.R. Sell, J.R. Allen, R.N. Day, M. Israelsson, M.W. Davidson, and J. Wang. 2013. A bright monomeric green fluorescent protein derived from Branchiostoma lanceolatum. *Nat Methods*. 10:407-409.

[6] Bajar, B.T., E.S. Wang, A.J. Lam, B.B. Kim, C.L. Jacobs, E.S. Howe, M.W. Davidson, M.Z. Lin, and J. Chu. 2016. Improving brightness and photostability of green and red fluorescent proteins for live cell imaging and FRET reporting. *Sci Rep*. 6:20889.

Supp. Table 4. Oligonucleotides used in this study

Target Region	Short Description	Sequence
UBA1	probe 1-fw	GTATGGTTTCAGACATCGAGC
UBA1	probe 1-rv	AGACTTGAATGAGATTTTACG
UBA1	probe 2-fw	CCAACGCTCTAGACAATGTCG
UBA1	probe 2-rv	CGGAATCAGTGAAGTAACCTTG
TIF35	probe fw	GATTGAGTAGGAACTGGAAACAAGC
TIF35	probe rv	CATACTGCCCTGGGATGGAACC
TAH11	probe 1-fw	TGACACGAGTCAAGGTTTTGATG
TAH11	probe 1-rv	GTCGCATAATGAGAGGTGCTG
TAH11	probe 2-fw	CCACCAGAGCTGCACGTTTTG
TAH11	probe 2-rv	TGGAAGCTATCACTTGTTGGTAC
POL3	probe fw	GTCCTGGATAACATTACCAAAAGG
POL3	probe rv	AGCAATACTCACAACGTTGGC
MCM7	probe 1-fw	AGTTTCTCCAGGGCACACAG
MCM7	probe 1-rv	ACGCATCATTCATGGAAGAGG
MCM7	probe 2-fw	ACCTCGAGGAGTGTATACCAC
MCM7	probe 2-rv	CCGCTAAGATTGAGGTTCTG
LCP5	probe fw	CTCGCTCACTGCGACATCAG
LCP5	probe rv	CGTTCACGTGCATCCATAGC
KAR2	probe fw	GGCACTAAGGTTACCCATGC
KAR2	probe rv	AGTGGCTTGGACTTCGAAAAC
PRE7	probe fw	TACTACGTTCATACGATCATTGC
PRE7	probe rv	AAGTGAACGAGTCTCTCACCAG
ACT1	probe 1-fw	CAAGACACCAAGGTATCATGGTC
ACT1	probe 1-rv	CTCTGTTTGATTTAGGGTTCATTG
ACT1	probe 2-fw	AAATCCTACGAACTTCCAGATG
ACT1	probe 2-rv	TTGCATTCTTTCGGCAATAC
ATP6	probe fw	TGGTTCAAGATGATTAATTTCACAAG
ATP6	probe rv	AATAACCATTAATAAATGACCAGCTAAG
COX3	probe fw	TTAGAAAGAAGTAGACATCAACAACATC
COX3	probe rv	TAATAAAGGTAATTCGGTAGGTTGTAC
COX1	qPCR fw*	CTACAGATACAGCATTTCCAAGA
COX1	qPCR rv*	GTGCCTGAATAGATGATAATGGT
ACT1	qPCR fw	CACCCTGTTCTTTTGACTGA
ACT1	qPCR rv	CGTAGAAGGCTGGAACGTTG

* Taylor, S.D., H. Zhang, J.S. Eaton, M.S. Rodeheffer, M.A. Lebedeva, W. O'Rourke T, W. Siede, and G.S. Shadel. 2005. The conserved Mec1/Rad53 nuclear checkpoint pathway regulates mitochondrial DNA copy number in Saccharomyces cerevisiae. *Mol Biol Cell*. 16:3010-3018.

Appendix A: Initial genetic analysis of Mrx6 and Pim1

In the previous chapter, we showed that Mrx6 negatively regulates mtDNA levels and deletion of *MRX6* increases mtDNA copy number. Given the biochemical interaction between Mrx6 and Pim1, one plausible hypothesis is that Mrx6 could regulate proteolytic activity of Pim1. To address the role of Mrx6-Pim1 interaction in regulating mtDNA copy number, we deleted *MRX6* and *PIM1* genes in the same strain. However, determining mtDNA levels in a Δ*pim1* strain is not straightforward, because Δ*pim1* cells lose intact mtDNA (Suzuki et. al., 1994; van Dyck et al., 1994; van Dyck et al., 1998). We similarly observed loss of mtDNA in the library strain in our colony blot screen (Supp. Table 1.2). Furthermore, generation of fresh *PIM1* deletions in WT or Δ*mrx6* cells followed by qPCR analysis of mtDNA levels in different clones yielded inconclusive results, with different clones displaying widely varying levels of mtDNA (Supp. Fig. 10A). The instability of mtDNA in Δ*pim1* cells is likely explained by pleiotropic effects, as Pim1 is the major Lon-type protease in mitochondria.

Next, we performed overexpression studies with Pim1 to examine its role in mtDNA copy number regulation. Overexpression of Pim1 reduced mtDNA levels in WT cells, as well as Δ*mrx6* cells (Supp. Fig. 10B). These observations are in line with our suggested role of Mrx6 as an adaptor conferring substrate specificity to Pim1. Overexpression of Pim1 could circumvent the need for such a specificity factor. However, overexpression of the protease could also create pleiotropic effects leading loss of mtDNA, making it difficult to arrive at a solid conclusion.

Our work elucidates, for the first time, an interaction partner of a Lon protease modulating mtDNA levels. However the mechanistic understanding of Mrx6 function remains unresolved, in particular whether Mrx6 acts through Pim1-mediated proteolysis to regulate mtDNA levels. Future studies on this subject would be invaluable to improve our understanding of mtDNA copy number control.

References:

Suzuki, C. K., K. Suda, N. Wang, and G. Schatz. 1994. Requirement for the yeast gene LON in intramitochondrial proteolysis and maintenance of respiration. *Science.* 264: 273LP-276.

van Dyck, L., D. A. Pearce, and F. Sherman. 1994. *PIMl* Encodes a Mitochondrial ATP-dependent Protease That Is Required for Mitochondrial Functionin the Yeast *Saccharomyces cerevisiae*. *J Biol Chem*. 269:238-242.

van Dyck, L., W. Neupert, and T. Langer. 1998. The ATP-dependent PIM1 protease is required for the expression of intron-containing genes in mitochondria. *Genes Dev*. 12:1515-1524.

Supp. Figure 10

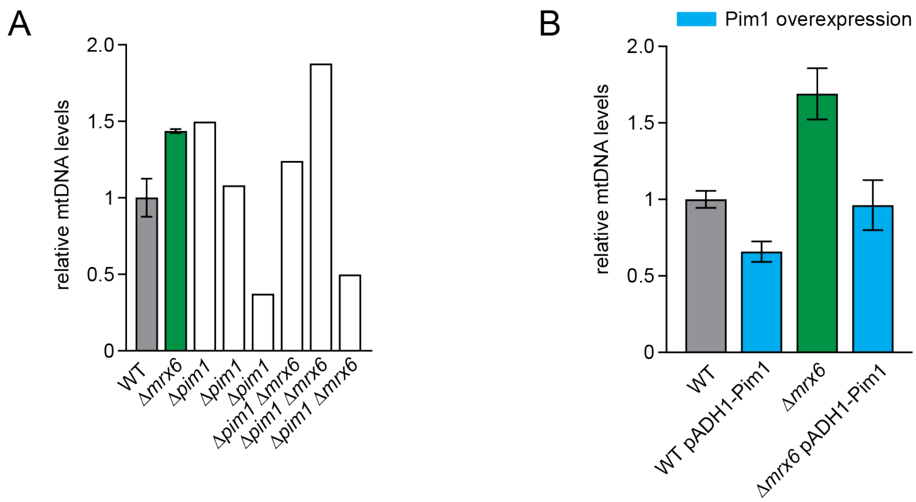

Supplementary Figure 10: mtDNA levels in the absence or overexpression of Pim1

A) qPCR analysis of mtDNA copy number in cells lacking *PIM1* and/or *MRX6.* (n=2 for WT and Δ*mrx6).* Cells were grown in YPD.
B) qPCR analysis of mtDNA copy number in cells overexpressing Pim1 (n=5). Cells were grown in SD-ura.

Publishing Agreement

It is the policy of the University to encourage the distribution of all theses, dissertations, and manuscripts. Copies of all UCSF theses, dissertations, and manuscripts will be routed to the library via the Graduate Division. The library will make all theses, dissertations, and manuscripts accessible to the public and will preserve these to the best of their abilities, in perpetuity.

Please sign the following statement:

I hereby grant permission to the Graduate Division of the University of California, San Francisco to release copies of my thesis, dissertation, or manuscript to the Campus Library to provide access and preservation, in whole or in part, in perpetuity.

Author Signature

03/20/2019

Date